UNITED STATES DEPARTMENT OF THE INTERIOR

GEOLOGICAL SURVEY

Geology, Geochemistry, and Mineralogy of the Ridenour Mine Breccia Pipe, Arizona

by

Karen J. Wenrich[1], Earl R. Verbeek[1], Hoyt B. Sutphin[2],
Peter J. Modreski[1], Bradley S. Van Gosen[1], and David E. Detra[1]

Open-File Report 90-0504

This study was funded by the Bureau of Indian Affairs
in cooperation with the Hualapai Tribe.

1990

This report is preliminary and has not been reviewed for conformity with U.S. Geological Survey editorial standards and stratigraphic nomenclature.

[1]U.S. Geological Survey
Denver, Colorado

[2]U.S. Pollution Control, Inc.
Boulder, Colorado

CONTENTS

ILLUSTRATIONS

ILLUSTRATIONS, continued

TABLES

Geology, Geochemistry, and Mineralogy of the Ridenour Mine Breccia Pipe, Arizona

Karen J. Wenrich, Earl R. Verbeek, Hoyt B. Sutphin,
Peter J. Modreski, Bradley S. Van Gosen, and David E. Detra

ABSTRACT

The Ridenour mine is located on the Hualapai Indian Reservation, northwestern Arizona, within the arcuate ring-fracture zone of a mineralized solution-collapse breccia pipe. Dissolution of the underlying Redwall Limestone in Late Mississippian time and subsequent collapse from above formed the Ridenour pipe and its associated ring fractures before any regional fracturing of the post-Redwall strata took place. Early solutions migrating through the pipe altered the normally reddish-orange Permian Esplanade Sandstone, within which the mine is located, to a pale pink, tan, or white color adjacent to the pipe core (now largely eroded). Subsequent solutions deposited Cu-V-U minerals under reducing conditions within the pipe and its surrounding ring-fracture zone; the pipe has been mined for all three metals at various times. Following mineralization the pipe and its surrounding host rocks were cut by five sets of joints and the pipe ores were highly oxidized. The regional fracture network of the Esplanade Sandstone, though complex, had no influence on ore distribution or grade, and the joints contain only local, patchy coatings of secondary Cu-V-U minerals derived from nearby ring fractures.

The Ridenour pipe, in common with most other mineralized breccia pipes of the Colorado Plateau in northern Arizona, contains anomalously high concentrations of Ag, As, Co, Cu, Mo, Ni, Pb, U, and Zn, but it differs from them in its exceptional enrichment in V and Ag. The average V content of 21 samples is 2.2%, and that of Ag is 400 ppm. Such enrichment is unknown from the primary (reduced) ore of breccia pipes on the North Rim, and only minor enrichment has been documented in two primary orebodies on the South Rim, one of them the Orphan mine. Both elements, however, are consistently enriched in the oxidized zone over breccia pipes, including those sampled over the North Rim orebodies; the high V and Ag contents of the oxidized Ridenour ores thus almost certainly are due to secondary enrichment through oxidation.

Oxidation at the Ridenour pipe has been so extensive that the primary ore minerals, such as uraninite, pyrite, chalcopyrite, bravoite, galena, and sphalerite, all of which are common in reduced ore from other pipes, have almost been totally removed from the Ridenour pipe. Only trace amounts of residual pyrite and galena have been observed. Supergene minerals, in approximate order of decreasing abundance, include malachite, azurite, goethite, hematite, roscoelite, tyuyamunite, metatyuyamunite, volborthite, calciovolborthite, conichalcite, vesignieite, naummanite, and argentite. The high vanadium content of most of the rocks is due to the presence of roscoelite, which replaced the normal dolomitic cement in the sandstone matrix.

The Ridenour pipe appears to be an oxidized version of the uranium-rich Orphan mine. The geochemistry and stratigraphic controls on the ore are identical. Extending the analogy, there appears to be little potential for an economic uranium orebody at the Ridenour mine because the ore zone in the Esplanade is oxidized, and the underlying Wescogame Formation at the Orphan mine did not yield much ore. In contrast, the average vanadium content at the

Ridenour mine is 10 times that of uranium, and hence, may have potential as an economic commodity.

INTRODUCTION

The Ridenour mine is one of about 35 old copper mines scattered throughout the Grand Canyon region of northern Arizona. The finely-tuned eyes of 19th century prospectors roaming the canyons in search of wealth missed few surface exposures of malachite or azurite along the stepped cliffs bordering the canyons of the Colorado River and its tributaries. Most, though not all, of these old copper mines were located within solution-collapse breccia pipes; among them was the Ridenour mine. The initial discovery of copper at the Ridenour breccia pipe occurred sometime during the 1870's (Miller, 1954).

The Ridenour mine sits 2800 ft above the Colorado River at the head of an unnamed tributary canyon located about 2 miles southeast of the river (fig. 1). The pipe is located along the west side of the canyon in a distinct amphitheather that formed by erosion of the pipe core up to the pipe ring fracture zone. Such erosion of Grand Canyon breccia pipes into amphitheaters is common and constitutes one criterion by which they can be recognized. Also assisting in pipe recognition is the common and conspicuous bleaching (reduction of ferric iron) of strata bordering the pipes as well as the breccia within the pipes; at the Ridenour mine the normally reddish-orange Esplanade sandstone (fig. 2) has been bleached to a bone-white color that is visible from miles away.

The Ridenour breccia pipe, like thousands of others in northern Arizona, is the result of cavern formation within the Mississippian Redwall Limestone, followed or accompanied by collapse (aided by solution weakening) of the overlying strata. This ultimately resulted in a nearly vertical, pipelike body filled with partially disaggregated collapse rubble, which was later cemented by carbonate and/or precipitation of ore minerals from mineralizing fluids. This pipelike body is in sharp contact with the normally flat-lying country rock. At no level in any pipe have breccia clasts been observed from lower units; all material has been dropped into them from stratigraphically higher units. The amount of minimum downdrop at the Esplanade level in the Ridenour mine--450 ft--is similar to that of documented clast displacements in other pipes, such as the Kanab North pipe, where Moenkopi strata have dropped over 700 ft, and the Orphan pipe, where clasts of Coconino strata have been observed 370 ft below their normal stratigraphic position (fig. 2). The accumulated clasts are characteristically poorly sorted, partly rounded due to solution, and embedded in a sandy to silty matrix that represents the insoluble component of clastic rocks that were once cemented by calcite and/or dolomite.

Mineralized breccia pipes of the southwestern Colorado Plateau are enriched in a large suite of elements. In addition to the metals U, Cu, Pb, Zn, and Ag, all of which have been recovered from various breccia pipes in the past, mineralized rock is also enriched in As, Ba, Cd, Co, Mo, Ni, Se, and V. The ores are texturally complex and the product of several related episodes of mineralization. Fluid-inclusion studies of sphalerite, calcite, and dolomite yielded temperatures ranging between 80°C and 173°C with salinities consistently >9 wt. % NaCl equivalent, although most commonly >18 wt.% NaCl equivalent (Wenrich and Sutphin, 1989). The main uranium-mineralizing event occurred at roughly 200 Ma, based on a large set of U-Pb

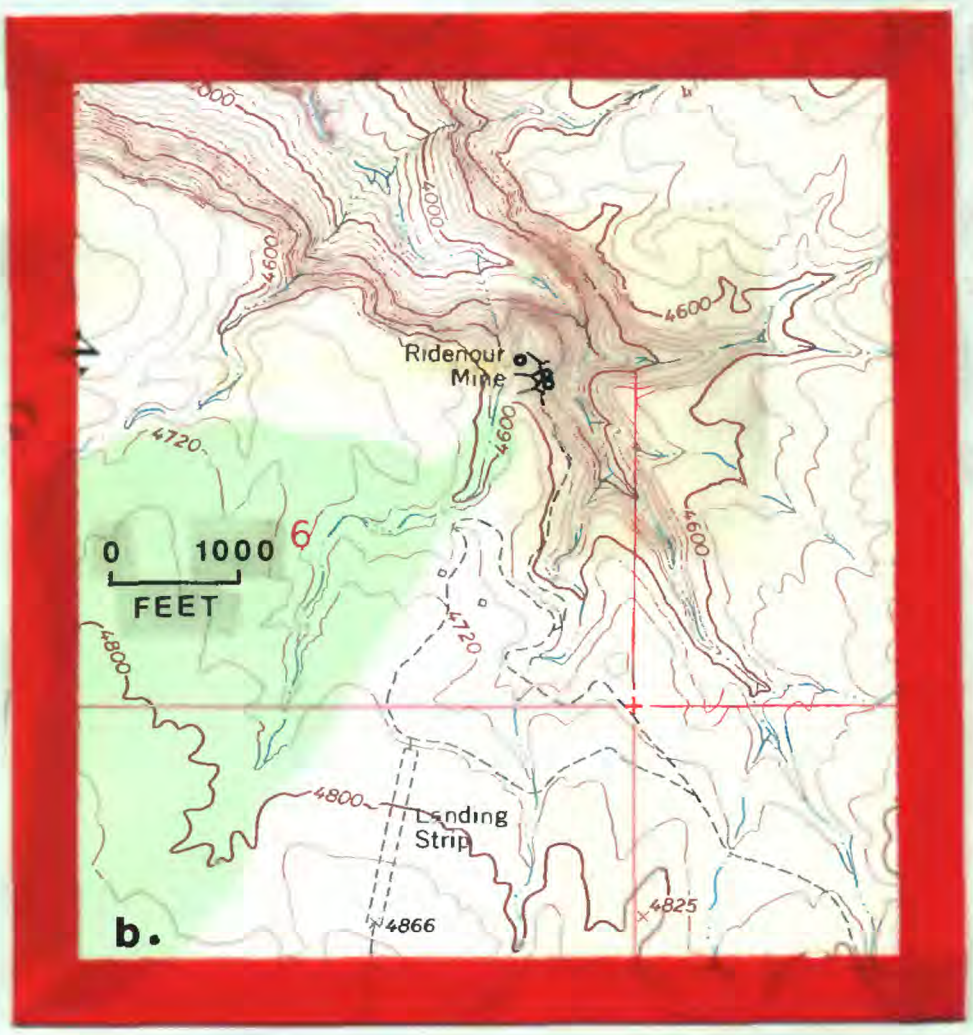

Figure 1. **a.** Index map of Arizona showing the location of the Hualapai Indian Reservation; the white square within the Reservation shows the location of figure 1b. **b.** Map showing the location of the Ridenour mine on the Vulcans Throne SW 7½ minute quadrangle. Adit symbols show the locations of the largest adits and the small circles mark drill hole locations. Note how the mine is located within an amphitheater--typical erosion for a breccia pipe.

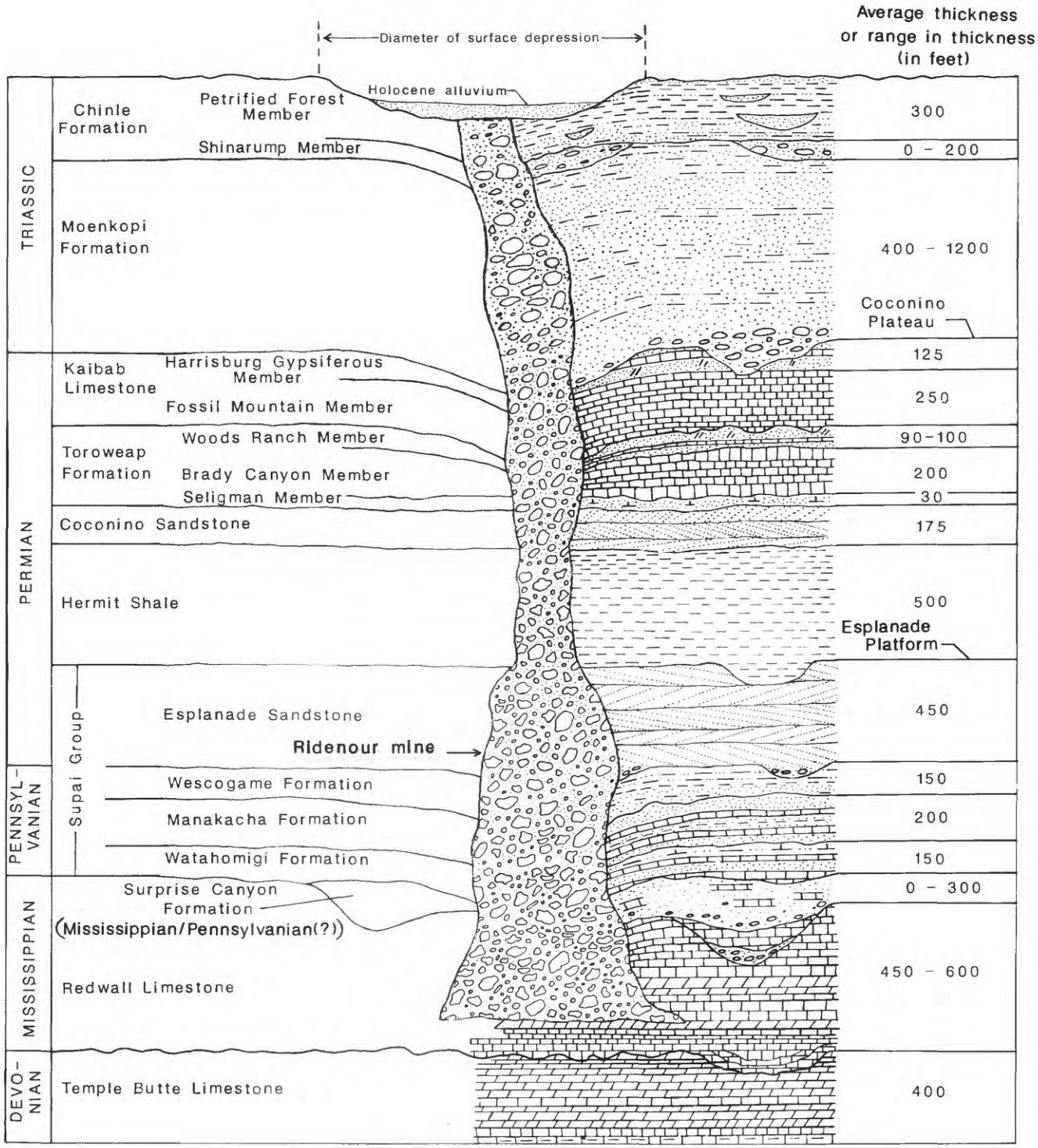

Figure 2. Vertical section through a typical solution-collapse breccia pipe. Thicknesses of units shown (from Wenrich and others, 1986) are for the northeastern Hualapai Indian Reservation. The stratigraphic position of the highest workings of the Ridenour mine is shown.

isotopic analyses from the Hack 2, Hack 3, Pigeon, Kanab North, EZ-1, EZ-2, and Arizona 1 breccia pipes (Ludwig and Simmons, 1988). However, data from the Canyon and Pinenut pipes indicate at least one earlier period of mineralization at roughly 260 Ma (Ludwig and Simmons, 1988).

The first record of a claim at the Ridenour breccia pipe was made in 1880 for copper and silver; production began in 1887 and continued intermittently until 1916 (Chenoweth, 1988). No records of production prior to 1904 have been found, but from 1904-1929 approximately 816,000 pounds of copper, 6,000 ounces of silver, and 39 ounces of gold were produced (Chenoweth, 1988). The only known uranium production on the Hualapai Reservation came from the Ridenour mine in 1961. During an Atomic Energy Commission (AEC) uranium reconnaissance survey of the Hualapai Indian Reservation, Miller (1954) estimated that reserves at the mine, in addition to the copper ore still in place, included 50 tons of uranium-vanadium ore averaging 0.38 percent U_3O_8 and 5.10 percent V_2O_8. Nevertheless, the 59 mi distance to Peach Springs and 2000 ft climb to the canyon rim made economic transport of the ore difficult, so that during the uranium boom of the 1950's there was apparently little or no activity at the mine. Finally, in 1961, 14 tons of ore, averaging 0.15 percent U_3O_8 and 2.36 percent V_2O_8 were shipped (Chenoweth, 1988), but thereafter production ceased. During 1976 three holes were drilled into the Ridenour pipe by Western Nuclear, Inc. who had obtained a lease from the Hualapai Tribe. The results were not encouraging and the lease was dropped in 1978. Drilling records for these holes are on file in the Hualapai Tribal office.

GEOLOGY AND STRUCTURE OF THE RIDENOUR MINE

The Ridenour pipe forms an amphitheather (fig. 3) from the Esplanade Platform, which at this location is 150 ft below the top of the Esplanade Sandstone, down 320 ft to the canyon floor; the canyon floor is well into the Wescogame Formation. The mine dump overlies the contact between the two formations, but the mine workings themselves are confined to the lower part of the Esplanade Sandstone (figs. 2 and 3). The central core of the breccia pipe is approximately 300 ft in diameter and the surrounding ring-fracture zone averages about 70 ft wide, yielding a total diameter of about 440 feet for the area of disturbed rock--fractured and/or brecciated--at the Ridenour pipe.

The 230 ft of pipe presently exposed probably represents only about one-fourth of the preserved vertical extent of the Ridenour pipe. Between the Esplanade and the Redwall Limestone, within which the pipe presumably bottoms, are 127 ft of Wescogame Formation, 168 ft of Manakacha Formation, and 178 ft of Watahomigi Formation (thicknesses from McKee, 1982--Whitmore Wash, Section 22a, located about 5 miles from the Ridenour Mine). Thus, this pipe has stoped upward from the Redwall Limestone through at least 500 ft of rock to where breccia can be observed in some of the lower mine workings. The original vertical extent of the Ridenour pipe cannot be determined because all rock overlying the Esplanade has been stripped by erosion. However, other pipes, where younger rocks are preserved, penetrate the entire Paleozoic section and extend into Lower Triassic strata; vertical extents of 1500-2500 ft appear not to be uncommon for these structures.

At the Esplanade level the eastern half of the Ridenour pipe, along with most of the pipe core have been removed by erosion; only the western part of the ring fracture zone is well preserved. Relatively little breccia is present in most of the mine workings, but a good exposure of the core breccia

A.

B.

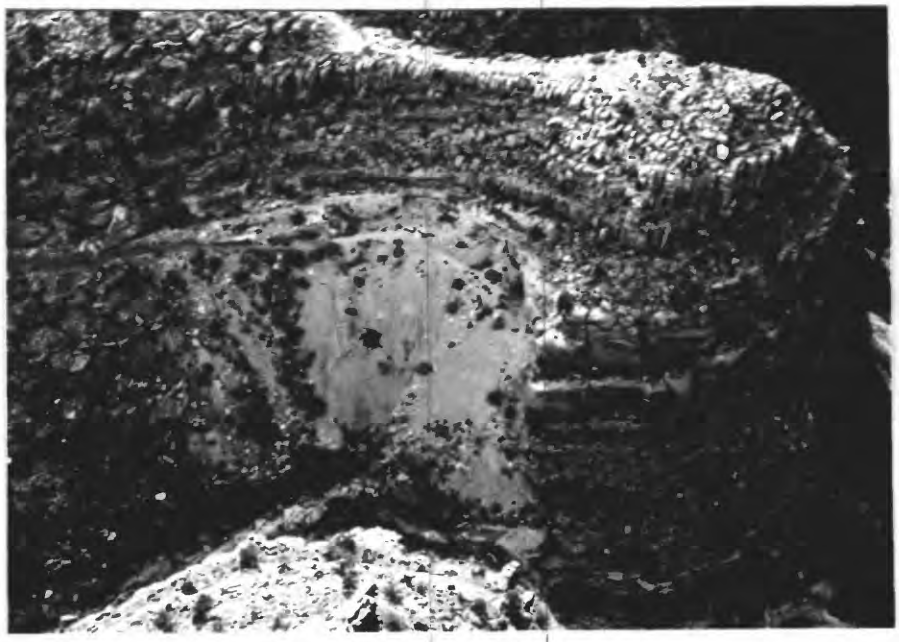

Figure 3. A. View from the top of the Coconino Plateau looking north toward the Ridenour mine (arrow). B. Aerial view of the Ridenour mine looking to the west-southwest. Note how the normally reddish-orange Esplanade Sandstone is bleached white. The core of the pipe has been eroded at this level leaving an amphitheather which follows the ring fracture zone. Most of the Cu-V-U ore lies within the ring fractures.

(fig. 4) exists along the main haulage adit beneath the road. Clasts of Hermit Shale have been observed within this breccia. The presence of these Hermit clasts at the stratigraphic level of the base of the Esplanade Sandstone shows downward movement of at least some clasts in the Ridenour pipe in excess of 450 ft, the approximate vertical distance between the haulage adit and the base of the Hermit Shale in nearby exposures.

Strata immediately surrounding the Ridenour pipe are unfaulted and in stratigraphic continuity with those farther distant but are cut by numerous, large fractures that strike everywhere approximately parallel to the pipe boundary and that dip outward at moderate angles averaging about 50°. These are the ring fractures, which formed during stoping and at the Ridenour mine occupy a zone varying in exposed width from about 40 to 130 ft. Early solutions migrating through the ring fractures widened them by dissolving carbonate cement from their sandstone walls to create irregular, lenticular voids, many of them filled with rubble derived by collapse of solution-weakened rock from the fracture walls (fig. 4). The rubble characteristically is embedded in a sandy matrix, the product of continued disaggregation of sandstone into loose grains, to form pockets of breccia superficially resembling the collapse breccia of the pipe core. The ring-fracture breccia differs from the core breccia, however, in that nearly all of it is monolithologic and contains clasts of only local derivation. The amphitheater at the Ridenour formed because of preferential erosion along the ring fracture zone. A detailed description of this ring fracture zone is provided by Verbeek and others (1988).

Within and for a few feet beyond the ring-fracture zone, the normally reddish-orange Esplanade Sandstone has been bleached to a pink, tan, or white color that visually accentuates the Ridenour amphitheater (fig. 3). This bleaching is due primarily to reduction of iron within the Esplanade and is not associated with any significant change in major element chemistry; the total iron content of the bleached versus unbleached rock shows little variation (Wenrich, 1986). The bleaching was an early and widespread effect, common to many pipes, and predated mineralization, which in most pipes was more local and affected lesser volumes of rock. At the Ridenour mine the dominant sites of mineralization were along the ring fractures, whose walls were coated with copper, vanadium, and uranium minerals, all later oxidized to various secondary phases. The same minerals and their later oxidation products also (1) coated sandstone clasts within the breccia pockets, (2) cemented the sandy matrix of the breccia, (3) filled residual pore space within the rock adjacent to the fracture walls and along the outer margins of breccia clasts, and (4) locally replaced the residual carbonate cement of the original rock. Most production from the Ridenour mine came from narrow, inclined stopes along the most thoroughly mineralized parts of the ring-fracture zone.

STRUCTURAL CONTROL OF THE RIDENOUR AND SIMILAR PIPES

Distinct alignments of breccia pipes, suggesting influence by underlying structure, occur in some areas of northwestern Arizona, while in others the pipes appear to be random (specifically throughout much of the Hualapai Reservation). Alignments are particularly striking on the Marble Plateau located about 85 miles east of the Ridenour mine. Maps of breccia-pipe locations in this area reveal nine distinct alignments along two preferred trends averaging N50°E and N45°W (Sutphin and Wenrich, 1983). However, the

Figure 4. Clast-supported collapse breccia filling a large solution pocket within the ring fracture zone. The clasts were not mineralized, but in this example the fine-grained matrix is colored bluish green due to the abundant malachite and azurite. Note the diffusion bands of limonite in the lower left corner of photograph (DB) and the bleaching of the clast margins (examples marked with a B).

parent formation of the pipes--The Redwall Limestone--is sparsely exposed and nearly inaccessible to study in this area, and so the question of structural control cannot be addressed satisfactorily by direct field evidence. Conversely, the Redwall Limestone is well exposed over parts of the Hualapai lands, but maps of known and suspected breccia pipes in the Redwall and younger strata for that region (Billingsley and others, 1986; Wenrich and others, 1986) reveal few convincing alignments of pipes. The reason probably is two-fold: (1) The Permian Kaibab and Toroweap Formations beneath the Hualapai lands contain thick, areally extensive layers of gypsum that have locally dissolved to produce collapse features morphologically similar to breccia pipes at the surface. The presence of these shallow-seated features in areas where Permian and younger rocks are preserved complicates attempts to recognize the more deeply rooted breccia pipes, and thus tends to conceal details of their distribution. The gypsiferous strata pinch out eastward, however, and are not present beneath the Marble Plateau; consequently the process of identifying breccia pipes in that area is inherently more simple and the pipe maps correspondingly more accurate. (2) Known and suspected breccia pipes in a few places on the Hualapai Reservation are sufficiently abundant and closely spaced that lines connecting pipes can be drawn in diverse directions much as one might draw numerous but meaningless connections between stars in the nighttime sky. Some of these apparent alignments, particularly the shorter ones, likely are fortuitous and unrelated to subsurface structure; their presence clouds attempts to recognize which among the possible alignments have true structural significance.

Little obvious evidence exists in surface and near-surface exposures in and around the Ridenour mine to suggest that the location of the Ridenour pipe was influenced by pre-existing structure. Nevertheless, the pipe is one of four pipes (identified by numbers 223, 243, 244, and 252 in Wenrich and others, 1986), that lie along a N45°E trend and that, unlike most other pipes in their vicinity, are conspicuously mineralized at the surface (Wenrich and others, 1986). The presence of such minerals as malachite, azurite, pyrite, and various secondary uranium minerals on surface exposure within pipes that lie along alignments suggests that the pipes were hydrologically connected and shared a common mineralization history in contrast to unaligned pipes in the area, none of which show evidence of mineralization. The nearby Lava Fault, also of N45°E trend and located 1.5 mi NW of the pipes, strengthens the supposition that the pipe alignment is real and related to pre-pipe structure. The Lava Fault cuts Permian through Cambrian strata and has 400 ft of offset, increasing southwestward to where it merges with the Hurricane fault system (Billingsley and others, 1986). It almost certainly is one of those faults, such as the Hurricane, of Precambrian ancestry and repeated movement. The possibility that Paleozoic movement on such faults influenced early fracture of the Redwall Limestone is a recurring theme in attempts to explain structural control of aligned breccia pipes (Sutphin and Wenrich, 1983; Wenrich and Sutphin, 1989).

Recent mapping of joints in Redwall and post-Redwall strata on the Hualapai Reservation has clarified some aspects of this process. In two regional studies, Roller (1987, 1989) found that the two oldest sets in the Redwall Limestone trend about N50°E and N45°W, parallel to the trends of aligned pipes on the Marble Plateau farther east and to the trend of the four mineralized pipes, including the Ridenour, discussed above. These early joints are present over a large area in nearly every Redwall outcrop studied, but were found neither by Roller, (1987, 1989) nor by Verbeek and others (1988) in any of the post-Redwall strata, including the Pennsylvanian

limestones of the Watahomigi Formation of the basal Supai Group immediately above the Redwall unconformity (fig. 2). The joints are thus of pre-Supai age. Within the Redwall Limestone are fracture-controlled, NE- and NW-trending cave passages, some of them partly filled with Late Mississippian sediments (the Surprise Canyon Formation) deposited by streams coursing through the cave system (Billingsley, 1986). These relations further constrain the time of fracture to a period of minor uplift in Late Mississippian time, during which the Redwall was emergent and stream valleys were cut into its surface. The structural control of the NE- and NW-trending cave passages in the Redwall is repeated in the alignments of pipes derived from them (Wenrich and Sutphin, 1989). Further, if fracture of the Redwall were not uniform, but had been more intense adjacent to pre-existing faults reactivated during the Late Mississippian episode of uplift, enhanced cave development and subsequent lengthy chains of pipes along these trends might be expected. Minor reactivation of faults during this time period has been documented in the Grand Canyon region (McKee and Gutschick, 1969; Huntoon, 1970; Huntoon and Sears, 1975), and both short and long alignments of pipes parallel to early fracture sets in the Redwall are observed. This is apparently due to preferential dissolution of the Redwall along these fracture trends. Apparently, pre-Supai group dissolution of the Redwall produced the bulk of the karst that formed mineralized breccia pipes. This suggested mechanism of structural control fits all known facts, and provides one ready explanation of how multiple pipes connected to the same cave system could have nearly identical mineralization histories.

The structural fabric developed during Mississippian time appears important to the genesis of the breccia pipes, whereas the fabric developed in later time appears unimportant. Lower Permian strata of the Esplanade Sandstone around the Ridenour pipe are cut by five regional sets of joints (Verbeek and others, 1988), but, in contrast to the Late Mississippian fracture network of the Redwall, these later sets were of no consequence to pipe genesis or mineralization. Abundant evidence exists at the Ridenour mine to show that the pipe stoped upward through unbroken rock and that the ring fractures surrounding it were the only fractures in existence when the ore minerals were deposited along them. That evidence, discussed at length in Verbeek and others (1988), includes the following observations: (1) joints cutting well-cemented parts of the collapse breccia in the pipe core can be matched to joint sets in undisturbed country rock around the pipe; (2) individual Esplanade clasts within the core breccia are not bounded by planar faces suggestive of jointing prior to brecciation; (3) the ring fractures were widened appreciably by dissolution as the pre-ore and ore fluids migrated through them, but the later joints do not show such solution-widening; (4) abutting relationships among the various fractures show that all five sets postdate the ring fractures; and (5) the ring fractures are mineralized but the joints are not, except for thin films of secondary minerals deposited by oxidizing ground waters. The work of Roller (1987, 1989) suggests that the five joints sets found in the Esplanade Platform are of relatively young geologic age, in that counterparts to them can be found, based on similarity in strikes and relative-age relations, in the Miocene Peach Springs Tuff (18 Ma, Damon, 1968) on the Hualapai Indian Reservation. However, Quaternary basalts (1.0-0.75 Ma, McKee and others, 1968) in the Vulcans Throne area, about 10 mi northeast of the Ridenour mine, do not contain the five regional sets of joints that occur in the Esplanade Sandstone at and nearby the Ridenour mine (Roller, 1989). This suggests that these five sets of joints formed between 18 Ma and 1 Ma, long after the formation and primary

mineralization of the Ridenour pipe.

Thus, the timing of geologic and structural events relevant to the formation of the Ridenour breccia pipe can be summarized as follows: (1) development of N50°E and N45°W fractures in the Redwall Limestone; (2) karstification of the Redwall Limestone; (3) deposition of the Pennsylvanian and Permian sediments; (4) collapsing of these Pennsylvanian and Permian sediments into the underlying Redwall cave system with the consequent formation of the ring fracture zone in the country rock enclosing the breccia core--much of the carbonate cement within the Pennsylvanian and Permian clastic sediments was dissolved, and some of the loose insoluble clastic debris was probably flushed through the cave system; (5) mineralization of the breccia matrix and ring fractures; and (6) jointing of the Pennsylvanian/Permian rock.

MINE WORKINGS

The bulk of the mine workings consist of arcuate drifts and associated narrow stopes that follow the most strongly mineralized portions of the ring fracture zone (fig. 5) along the west side of the pipe (fig. 6). Copper-, vanadium-, and uranium-bearing minerals can still be seen filling parallel ring fractures in these areas. Chenoweth (1988) provides a good description of the mine workings: "The old copper workings extend around the perimeter of the pipe for nearly 500 feet [fig. 6]. Here, ore in the ring fracture zone has been mined for a vertical distance of over 80 feet. The main level of the mine is about 100 feet below the exposed top of the pipe and was reached by two inclined shafts and a haulage adit whose portal is blocked by dump material. The upper stopes have access holes to the surface, and the remaining workings consist of short prospect adits and small open cuts."

The mine was first mapped by Miller (1954), whose map is still reasonably accurate except along the northern edge of the pipe, near the no. 3 adit, where renewed mining altered some of the older workings and subsequent collapse rendered portions of them inaccessible. For the most part, however, the workings remain open. The arcuate drift following the ring fracture zone near the surface is still negotiable, though tight crawls over piles of rubble are necessary in places, and the lower level at 4428 ft can still be reached by descending either the inclined shaft along the road near the no. 1 adit (fig. 6) or the 40° ramp (formerly a winze, now much stoped) between it and the 4480 ft level within the mine. Because most of the stopes follow the ring fractures, which average only about 50° in dip, they too can easily be climbed to the uppermost level of the mine except in areas of backfill. The stoping of the orebody along the ring fractures is so extensive that much of the cliff along the outer edge of the pipe appears as if hollow.

GEOCHEMISTRY

The Ridenour pipe is similar to most other mineralized breccia pipes in northern Arizona in that it contains anomalous concentrations of Ag, As, Co, Cu, Mo, Ni, Pb, U, and Zn. Table 1 shows the analytical results for 21 samples collected from the Ridenour mine at locations shown in figure 6, and analyzed according to the procedures described in Appendix A. Petrographic descriptions of these and additional samples are provided in Appendix B. The combined effects of mineralization and later oxidation on the chemistry of the

Figure 5. A. The Cu-U-V minerals precipitated along the breccia-pipe ring fractures (see arrow) and hence the mine adits and stopes follow the fractures, as can be seen in this photo. The dark bands lying at about 45° are Cu-U-V-filled ring fractures. B. Later vertical joints (J2 or J3 set of Verbeek and others, 1988) cutting vanadium-mineralized ring fractures (see arrow) that dip away from the observer. Some of the vertical joints appear filled, but they are "unmineralized"--the filling is merely caliche.

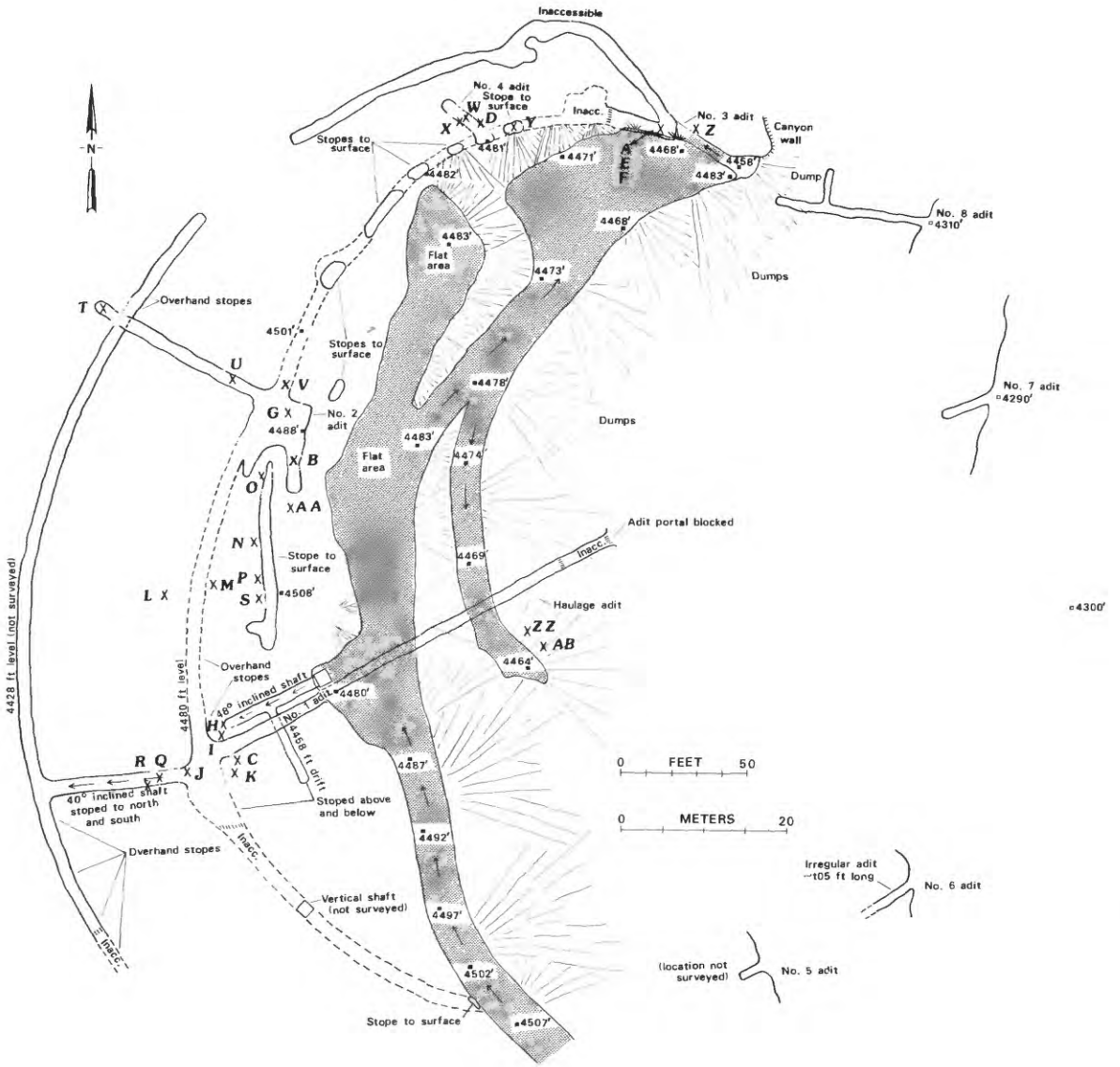

Figure 6. Map of the mine workings (modified from Verbeek and others, 1988 and Miller, 1954) and sample localities. The sample localities are designated with an "X" and a letter. The letter(s) corresponds to the middle digit(s) (between the hyphens) of the sample numbers shown in table 1 and appendix 1. Samples with the same letter, but with a trailing number, represent multiple samples from the same site (within 5 feet).

Table 1 -- Chemical analyses of samples collected from the Ridenour mine breccia pipe.[1]

Field ID	Ag ppm ICP	Al % ICP	Al2O3 % XRF	As ppm AA	As ppm ICP	Au ppm AA	Au ppm ICP	Ba ppm ICP	Ba ppm NA	Be ppm ICP	Bi ppm ICP	C % (Crbnt)
*223-A-C82	20.	4.9	-H-	2100.	2500.	<0.05	<20.	640.	900.	14.	<20.	0.010
*223-D-C83	<2.0	2.0	3.83	—	100.	—	<8.0	400.	410.	2.0	<10.	0.140
*223-E-C83	30.	3.8	(H) 6.71	790.	500.	<0.05	<40.	720.	—	87.	<50.	0.350
*223-F-C83	4.0	2.5	4.67	110.	80.	—	<8.0	380.	—	16.	<10.	0.020
*223-G-C83	140.	3.8	(H) 6.43	3200.	2400.	<0.05	<20.	200.	140.	120.	<20.	0.060
*223-P-C86	2400.	2.4	(H) 4.54	—	8100.	—	<8.0	2200.	3000.	<1.00	—	0.920
*223-Q-C86	40.	1.8	(H) 3.18	—	1300.	—	<8.0	2400.	2700.	<1.00	—	1.80
223-R-C86	76.	1.7	(H) 3.20	—	40.	—	<8.0	280.	240.	<1.00	—	0.520
*223-S-C86	2400.	2.1	-H-	—	15000.	—	<8.0	1200.	1800.	<1.00	—	0.760
*223-T-C86	5.0	1.6	2.72	—	80.	—	<8.0	250.	240.	<1.00	—	3.46
*223-W-C86	160.	1.9	(H) 3.55	—	4900.	—	<8.0	1600.	2100.	<1.00	—	0.060
223-W-C86R	130.	2.0	(H) 3.78	—	3900.	—	<8.0	1600.	2400.	<1.00	—	0.060
*223-Y-C86	400.	0.45	-H-	—	730.	—	<8.0	62.	140.	<1.00	—	3.58
*223-AA-C86	32.	3.8	(H) 11.3	—	480.	—	<8.0	160.	210.	<1.00	—	0.020
*223-M1-C86	<2.0	0.11	0.29	—	1300.	—	<8.0	20.	150.	<1.00	—	11.3
*223-N1-C86	2100.	1.2	(H) 2.25	—	3900.	—	<8.0	180.	380.	<1.00	—	0.880
223-N2-C86	280.	2.0	(H) 3.56	—	4400.	—	<8.0	300.	350.	<1.00	—	0.050
*223-U1-C86	<2.0	7.3	13.5	—	30.	—	<8.0	320.	340.	3.0	—	<0.010
*223-U2-C86	<2.0	7.8	14.2	—	20.	—	<8.0	310.	330.	3.0	—	1.19
*223-Z1-C86	27.	3.0	(H) 5.51	—	380.	—	<8.0	2800.	3000.	<1.00	—	1.18
*223-ZZ-C86	60.	1.3	(H) 2.28	—	1500.	—	<8.0	240.	280.	<1.00	—	1.98

[1]EXPLANATION:

Column 1 contains the sample identification number. The first three digits of the number identify the breccia pipe; the letter indicates sample location within the pipe (see figure 6 for exact locations), and the last 2 numbers indicate the year the sample was collected. Sample "223-W-C86R" is a replicate sample of "223-W-C86".

Other columns contain element concentrations; in the column header the first third indicates the element looked for (elements are listed in alphabetical order), the second indicates the units of concentration (%=percent; ppm=parts per million), and the last third indicates the analytical method used to determine element concentrations (ICP=inductively coupled plasma; ES = six-step semi-quantitative emission spectroscopy; XRF=X-ray fluorescence; AA=atomic absorption; NA=instrumental neutron activation analysis; and DN=delayed neutron analysis), except for C and S, where element form is indicated. "Crbnt" = carbonate; "Orgnc" = organic; "$FeTO_3$" = total iron expressed as Fe_2O_3; "LOI 900C" = loss on ignition at 900°C. A "<" symbol indicates that an element was below the limit of determination. A dash (-) means that element was not determined. An "H" indicates that there were matrix interferrences while analyzing this sample--commonly from high grade metals such as Cu--consequently these data are probably only semi-quantitative. An "N" indicates that no spectrographic line was observed for that element, as opposed to an "L" where a line was observed but the concentration was less than the detection limit.

* Petrographic description is provided in Appendix B.

Table 1 -- continued

Field ID	C % (Orgnc)	C % (Total)	Ca % ICP	CaO % XRF	Cd ppm ICP	Ce ppm ICP	Ce ppm NA	Co ppm ICP	Co ppm NA	Cr ppm ICP	Cr ppm NA	Cs ppm AA
223-A-C82	<0.010	<0.010	0.26	-H-	<4.0	56.	110.	210.	200.	14.	18.	8.0
223-D-C83	0.010	0.150	0.43	0.55	<2.0	17.	14.	31.	24.	17.	16.	—
223-E-C83	0.040	0.390	0.85	(H) 1.000	<10.	30.	—	120.	—	54.	—	6.0
223-F-C83	0.030	0.050	0.07	0.08	<2.0	23.	—	52.	—	28.	—	4.0
223-G-C83	0.040	0.100	0.40	(H) 0.49	<4.0	39.	42.	56.	45.	62.	17.	3.0
223-P-C86	0.030	0.950	0.15	(H) 0.20	<2.0	20.	<180.	480.	410.	11.	—	—
223-Q-C86	0.100	1.90	4.0	(H) 5.67	<2.0	<4.0	8.1	550.	540.	1.00	11.	—
223-R-C86	0.030	0.550	0.04	(H) 0.04	<2.0	7.0	<8.4	4300.	3300.	9.0	17.	—
223-S-C86	<0.010	0.750	0.21	-H-	<2.0	43.	<460.	890.	800.	4.0	<3.3	—
223-T-C86	0.010	3.47	7.1	9.54	<2.0	11.	—	12.	7.8	9.0	11.	—
223-W-C86	<0.010	0.040	0.79	(H) 1.14	<2.0	57.	<340.	1700.	1600.	5.0	—	—
223-W-C86R	<0.010	0.030	0.43	(H) 0.60	<2.0	75.	<310.	1400.	1200.	5.0	—	—
223-Y-C86	<0.010	2.63	0.05	-H-	<2.0	<4.0	<10.	430.	22.	4.0	22.	—
223-AA-C86	<0.010	<0.010	0.11	(H) 0.10	<2.0	4.0	<3.6	13.	11.	23.	23.	—
223-M1-C86	<0.100	11.0	38.	53.3	12.	<4.0	<4.0	270.	230.	2.0	2.8	—
223-N1-C86	0.030	0.910	0.45	(H) 0.57	<2.0	<4.0	<14.	1700.	1300.	13.	22.	—
223-N2-C86	<0.010	0.010	1.4	(H) 1.92	<2.0	110.	96.	1600.	1300.	<1.00	14.	—
223-U1-C86	<0.010	<0.010	0.15	0.20	<2.0	59.	57.	8.0	5.9	95.	86.	—
223-U2-C86	0.030	1.22	4.2	5.85	<2.0	61.	54.	9.0	4.8	90.	96.	—
223-Z1-C86	0.080	1.26	2.3	(H) 3.17	<2.0	11.	13.	120.	110.	5.0	18.	—
223-ZZ-C86	0.120	2.10	2.8	(H) 3.70	<2.0	<4.0	7.5	560.	490.	9.0	11.	—

Table 1 -- continued

Field ID	Cs ppm NA	Cu ppm ICP	Dy ppm ICP	Er ppm ICP	Eu ppm ICP	Eu ppm NA	F %	Fe % ICP	Fe % NA	FeTO3 % XRF	Ga ppm ICP	Gd ppm ICP
223-A-C82	7.6	5500.	30.	12.	13.	13.	0.060	0.52	0.522	-H-	13.	40.
223-D-C83	2.5	250.	—	—	<2.0	0.27	0.020	0.46	0.428	0.58	6.0	—
223-E-C83	—	1900.	<20.	<20.	<10.	—	0.050	0.48	—	(H) 0.41	80.	<50.
223-F-C83	—	510.	8.0	<4.0	3.0	—	0.030	0.25	—	0.29	23.	<10.
223-G-C83	2.8	8800.	19.	12.	—	10.	0.050	0.90	0.705	(H) 0.87	110.	<20.
223-P-C86	1.9	120000.	—	—	13.	12.	0.030	0.49	0.297	(H) 0.41	14.	—
223-Q-C86	1.9	89000.	—	—	<2.0	0.35	0.020	0.45	0.256	(H) 0.30	<4.0	—
223-R-C86	1.2	54000.	—	—	<2.0	0.17	0.010	0.22	0.218	(H) 0.32	10.	—
223-S-C86	8.0	170000.	—	—	22.	24.	0.030	0.69	0.383	-H-	21.	—
223-T-C86	1.0	390.	—	—	<2.0	0.42	0.020	0.31	0.269	0.38	<4.0	—
223-W-C86	4.4	32000.	—	—	14.	14.	0.030	1.00	0.769	(H) 1.05	10.	—
223-W-C86R	8.0	33000.	—	—	20.	19.	0.030	1.1	0.916	(H) 1.53	10.	—
223-Y-C86	0.46	530000.	—	—	<2.0	0.17	<0.010	1.5	1.34	-H-	24.	—
223-AA-C86	1.8	4700.	—	—	<2.0	1.4	0.030	0.57	0.358	(H) 0.47	8.0	—
223-M1-C86	0.093	3800.	—	—	<2.0	0.14	0.010	2.6	2.66	3.55	<4.0	—
223-N1-C86	0.84	110000.	—	—	<2.0	0.91	0.020	0.31	0.251	(H) 0.26	9.0	—
223-N2-C86	1.4	37000.	—	—	25.	24.	0.030	0.78	0.579	(H) 0.75	6.0	—
223-U1-C86	13.	94.	—	—	<2.0	0.65	0.110	4.0	4.08	5.83	17.	—
223-U2-C86	14.	150.	—	—	<2.0	0.65	0.110	1.5	1.53	2.23	19.	—
223-Z1-C86	2.7	12000.	—	—	2.0	2.3	0.020	0.54	0.328	(H) 0.38	<4.0	—
223-ZZ-C86	0.84	60000.	—	—	<2.0	0.32	0.010	2.4	2.39	(H) 3.27	7.0	—

Table 1 -- continued

Field ID	Gd ppm NA	Ge ppm ES	Hf ppm NA	Hg ppm AA	Ho ppm ICP	K % ICP	K2O % XRF	LOI 900C XRF	La ppm ICP	La ppm NA	Li ppm AA	Li ppm ICP
223-A-C82	43.	—	9.5	0.62	<8.0	3.1	-H-	-H-	9.0	23.	40.	40.
223-D-C83	—	—	7.1	0.08	<4.0	1.9	2.17	1.44	9.0	9.7	—	4.0
223-E-C83	—	—	—	0.30	—	2.6	(H) 3.21	(H) 2.67	<10.	—	16.	10.
223-F-C83	—	—	—	0.01	<4.0	1.8	2.36	1.09	9.0	—	9.0	7.0
223-G-C83	38.	—	8.2	6.0	—	2.7	(H) 3.40	(H) 1.90	5.0	4.5	22.	16.
223-P-C86	—	10.	9.9	80.	<4.0	1.8	(H) 2.20	(H) 6.96	3.0	57.	—	9.0
223-Q-C86	—	N10.	5.3	4.0	<4.0	1.4	(H) 1.65	(H) 11.1	2.0	5.0	—	5.0
223-R-C86	—	N10.	9.2	3.0	<4.0	1.6	(H) 1.87	(H) 4.34	6.0	6.7	—	4.0
223-S-C86	—	15.	7.4	60.	<4.0	1.9	-H-	-H-	3.0	230.	—	10.
223-T-C86	—	N10.	6.2	0.07	<4.0	1.6	1.65	13.7	6.0	6.5	—	5.0
223-W-C86	—	20.	6.9	2.0	<4.0	1.4	(H) 1.75	(H) 2.58	3.0	200.	—	15.
223-W-C86R	—	<10.	5.7	2.0	4.0	1.5	(H) 1.90	(H) 2.87	5.0	130.	—	12.
223-Y-C86	—	<10.	5.1	N2.0	<4.0	0.43	-H-	-H-	<2.0	8.6	—	2.0
223-AA-C86	—	<10.	6.3	0.80	<4.0	3.0	(H) 3.78	(H) 1.85	<2.0	3.4	—	12.
223-M1-C86	—	<10.	0.44	0.56	<4.0	0.05	0.05	42.1	<2.0	2.3	—	<2.0
223-N1-C86	—	N10.	5.9	N20.	<4.0	0.98	(H) 1.12	(H) 7.05	5.0	7.1	—	4.0
223-N2-C86	—	10.	5.5	N2.0	6.0	1.4	(H) 1.68	(H) 5.07	9.0	10.	—	34.
223-U1-C86	—	N10.	9.0	1.5	<4.0	4.0	4.67	4.89	30.	28.	—	37.
223-U2-C86	—	N10.	9.7	0.46	<4.0	4.2	4.66	9.55	30.	29.	—	36.
223-Z1-C86	—	N10.	9.8	0.40	<4.0	2.6	(H) 3.05	(H) 6.47	4.0	6.5	—	6.0
223-ZZ-C86	—	N10.	7.1	2.6	<4.0	1.2	(H) 1.40	(H) 9.41	3.0	4.7	—	5.0

Table 1 -- continued

Field ID	Lu ppm NA	Mg % ICP	MgO % XRF	Mn ppm ICP	MnO % XRF	Mo ppm ICP	Na % ICP	Na % NA	Na2O % XRF	Nb ppm ICP	Nd ppm ICP	Nd ppm NA
223-A-C82	1.00	0.52	-H-	21.	-H-	260.	0.07	0.072	-H-	26.	170.	100.
223-D-C83	—	0.20	0.34	25.	<0.02	23.	0.05	0.044	0.16	<4.0	10.	2.5
223-E-C83	—	0.72	(H) 1.15	<20.	<0.02	10.	0.08	—	<0.15	180.	—	—
223-F-C83	—	0.23	0.44	11.	<0.02	87.	0.07	—	<0.15	34.	32.	—
223-G-C83	0.55	0.35	(H) 0.64	<8.0	<0.02	56.	0.07	—	(H) 0.16	160.	—	69.
223-P-C86	—	0.22	(H) 0.44	8.0	<0.04	220.	0.02	<0.02	<0.30	—	51.	<160.
223-Q-C86	0.10	1.5	(H) 2.50	39.	<0.04	11.	0.09	0.078	(H) 0.30	—	<4.0	4.3
223-R-C86	0.11	0.13	(H) 0.30	11.	<0.03	9.0	0.09	0.085	<0.20	—	<4.0	2.9
223-S-C86	—	0.20	-H-	<4.0	-H-	47.	0.02	—	-H-	—	110.	<260.
223-T-C86	0.13	3.5	5.61	100.	<0.02	<2.0	0.06	0.045	<0.15	—	5.0	8.1
223-W-C86	—	0.20	(H) 0.41	5.0	<0.03	11.	0.03	0.085	<0.20	—	85.	<200.
223-W-C86R	—	0.20	(H) 0.36	8.0	<0.04	13.	0.03	—	<0.30	—	130.	<220.
223-Y-C86	—	0.06	-H-	<4.0	-H-	63.	0.02	0.024	-H-	—	<4.0	<4.2
223-AA-C86	0.094	0.35	(H) 0.67	7.0	<0.03	110.	0.03	0.029	<0.20	—	9.0	11.
223-M1-C86	—	0.30	0.53	110.	<0.02	13.	0.05	0.032	<0.15	—	<4.0	<2.3
223-N1-C86	0.11	0.33	(H) 0.60	7.0	<0.04	330.	0.20	0.18	(H) 0.40	—	<4.0	9.7
223-N2-C86	0.56	0.27	(H) 0.50	<4.0	<0.04	5.0	0.07	0.054	<0.03	—	160.	110.
223-U1-C86	0.41	1.00	1.79	95.	<0.02	<2.0	0.09	0.087	0.18	—	22.	22.
223-U2-C86	0.41	1.1	1.78	41.	<0.02	<2.0	0.12	0.095	<0.15	—	21.	21.
223-Z1-C86	0.25	1.4	(H) 2.36	38.	<0.03	4.0	0.05	0.043	<0.30	—	14.	17.
223-ZZ-C86	0.10	1.7	(H) 2.68	52.	<0.03	17.	0.04	0.036	<0.20	—	<4.0	3.9

Table 1 -- continued

Field ID	Ni ppm ICP	P % ICP	P2O5 % XRF	Pb ppm ICP	Pd ppb AA	Pr ppm ICP	Pt ppb AA	Rb ppm AA	Rb ppm NA	Rh ppb AA	Ru ppb AA	S % (Total)
223-A-C82	520.	<0.01	-H-	4200.	—	30.	—	120.	130.	—	—	<0.01
223-D-C83	74.	0.005	<0.05	61.	—	—	—	—	47.	—	—	<0.01
223-E-C83	260.	<0.03	<0.05	330.	—	<50.	—	94.	—	—	—	<0.01
223-F-C83	120.	<0.005	<0.05	810.	—	<10.	—	55.	—	—	—	<0.01
223-G-C83	250.	0.02	(H) 0.06	11000.	<8.0	30.	25.	96.	100.	45.	<5.0	<0.01
223-P-C86	1400.	0.006	<0.10	11000.	—	—	—	—	72.	—	—	0.09
223-Q-C86	600.	<0.005	<0.10	83.	—	—	—	—	44.	—	—	0.03
223-R-C86	3600.	<0.005	<0.07	55.	—	—	—	—	41.	—	—	0.03
223-S-C86	1300.	<0.005	-H-	13000.	—	—	—	—	100.	—	—	0.49
223-T-C86	19.	0.006	<0.05	88.	—	—	—	—	31.	—	—	<0.01
223-W-C86	1800.	<0.005	<0.07	6300.	—	—	—	—	71.	—	—	0.02
223-W-C86R	1300.	<0.005	<0.10	4300.	—	—	—	—	74.	—	—	0.02
223-Y-C86	440.	0.05	-H-	<4.0	—	—	—	—	17.	—	—	4.7
223-AA-C86	86.	<0.005	<0.07	6800.	—	—	—	—	92.	—	—	0.01
223-M1-C86	180.	0.01	<0.05	460.	—	—	—	—	3.4	—	—	0.11
223-N1-C86	3100.	<0.005	(H) 0.12	30000.	—	—	—	—	33.	—	—	0.07
223-N2-C86	2900.	0.007	<0.10	28000.	—	—	—	—	71.	—	—	0.03
223-U1-C86	49.	0.02	<0.05	29.	—	—	—	—	160.	—	—	0.01
223-U2-C86	52.	0.02	0.05	22.	—	—	—	—	160.	—	—	<0.01
223-Z1-C86	99.	0.009	<0.07	3100.	—	—	—	—	100.	—	—	0.02
223-ZZ-C86	2800.	<0.005	<0.07	370.	—	—	—	—	28.	—	—	0.01

Table 1 -- continued

Field ID	Sb ppm NA	Sc ppm ICP	Sc ppm NA	Se ppm AA	SiO2 % XRF	Sm ppm ICP	Sm ppm NA	Sn ppm ICP	Sr ppm ICP	Ta ppm ICP	Ta ppm NA	Tb ppm ICP
223-A-C82	2.9	6.0	6.8	6.8	-H-	50.	39.	<8.0	290.	<80.	<0.45	<40.
223-D-C83	1.1	<2.0	1.6	0.70	90.1	—	0.84	<20.	46.	<40.	0.36	—
223-E-C83	—	<10.	—	1.1	(H) 77.2	<50.	—	<20.	300.	<200.	—	<100.
223-F-C83	—	3.0	—	0.30	88.4	<10.	—	<4.0	41.	<40.	—	<20.
223-G-C83	5.4	5.0	3.8	5.7	(H) 74.1	30.	40.	<8.0	45.	<80.	0.27	<40.
223-P-C86	38.	3.0	3.7	2800.	(H) 61.2	—	54.	<20.	54.	<40.	0.37	—
223-Q-C86	3.4	<2.0	1.4	18.	(H) 57.3	—	1.1	<20.	57.	<40.	0.24	—
223-R-C86	2.0	<2.0	1.1	210.	(H) 81.7	—	0.65	<20.	38.	<40.	0.99	—
223-S-C86	32.	<2.0	3.2	3000.	-H-	—	76.	<20.	370.	<40.	0.71	—
223-T-C86	0.31	<2.0	1.4	3.8	65.9	—	2.0	<20.	42.	<40.	0.24	—
223-W-C86	13.	<2.0	3.0	95.	(H) 72.2	—	53.	<20.	630.	<40.	0.54	—
223-W-C86R	12.	<2.0	3.6	95.	(H) 75.8	—	73.	<20.	380.	<40.	0.55	—
223-Y-C86	2.7	<2.0	0.67	-H-	-H-	—	0.93	<20.	29.	<40.	0.15	—
223-AA-C86	3.8	3.0	3.2	13.	(H) 76.2	—	6.3	<20.	19.	<40.	0.24	—
223-M1-C86	3.7	<2.0	0.31	5.5	0.91	—	0.56	<20.	140.	<40.	—	—
223-N1-C86	4.1	<2.0	1.4	830.	(H) 68.0	—	2.7	<20.	110.	<40.	0.14	—
223-N2-C86	20.	3.0	3.9	130.	(H) 69.7	—	77.	<20.	650.	<40.	0.12	—
223-U1-C86	0.87	11.	12.	0.50	67.8	—	3.9	<20.	79.	<40.	1.3	—
223-U2-C86	0.56	11.	11.	0.20	61.0	—	4.0	<20.	83.	<40.	1.3	—
223-Z1-C86	2.6	2.0	2.5	54.	(H) 66.1	—	8.5	<20.	130.	<40.	0.39	—
223-ZZ-C86	1.5	<2.0	1.3	63.	(H) 69.2	—	1.9	<20.	37.	<40.	0.22	—

Table 1 -- continued

Field ID	Tb ppm NA	Th ppm DN	Th ppm ICP	Th ppm NA	Ti % ICP	TiO2 % XRF	Tm ppm NA	U ppm DN	U ppm ICP	U ppm NA	V ppm ICP	Y ppm ICP
223-A-C82	5.7	<1300.	24.	4.8	0.12	-H-	1.4	3100.	3000.	2600.	40000.	72.
223-D-C83	0.13	<330.	<4.0	2.0	0.12	0.22	—	910.	1000.	840.	1800.	4.0
223-E-C83	—	<690.	<20.	—	0.13	(H) 0.24	—	1800.	1700.	—	27000.	50.
223-F-C83	—	<250.	<4.0	—	0.11	0.23	—	610.	500.	—	5200.	19.
223-G-C83	4.6	<14.	<8.0	2.8	0.08	(H) 0.14	0.95	76.	<200.	74.	36000.	55.
223-P-C86	6.2	<1400.	<4.0	1.7	0.08	(H) 0.13	—	4100.	4200.	3600.	33000.	83.
223-Q-C86	0.17	<14.	<4.0	1.9	0.05	(H) 0.09	—	13.	<100.	7.8	46000.	12.
223-R-C86	0.14	<21.	<4.0	5.2	0.07	(H) 0.19	—	25.	<100.	24.	180.	4.0
223-S-C86	9.9	<7500.	<4.0	2.0	0.09	-H-	—	15000.	16000.	14000.	50000.	130.
223-T-C86	0.25	<41.	<4.0	1.8	0.05	0.15	—	83.	<100.	75.	170.	6.0
223-W-C86	6.6	<6700.	<4.0	2.7	0.07	(H) 0.13	—	14000.	15000.	13000.	43000.	88.
223-W-C86R	9.4	<4000.	<4.0	—	0.07	(H) 0.12	—	9900.	11000.	9800.	36000.	120.
223-Y-C86	0.15	<77.	14.	0.83	0.03	-H-	—	200.	200.	420.	320.	<2.0
223-AA-C86	0.60	<26.	<4.0	2.1	0.07	(H) 0.16	—	34.	<100.	35.	43000.	13.
223-M1-C86	0.078	<58.	<4.0	—	<0.005	<0.02	—	130.	100.	130.	380.	<2.0
223-N1-C86	0.44	<45.	<4.0	1.9	0.07	(H) 0.12	—	96.	100.	74.	12000.	10.
223-N2-C86	11.	<33.	<4.0	1.4	0.06	(H) 0.09	—	56.	<100.	45.	50000.	73.
223-U1-C86	0.50	11.	11.	11.	0.32	0.83	—	3.3	<100.	3.2	120.	8.0
223-U2-C86	0.54	14.	10.	11.	0.34	0.88	—	4.7	<100.	4.6	94.	10.
223-Z1-C86	1.3	<18.	<4.0	2.6	0.11	(H) 0.24	—	17.	<100.	18.	50000.	27.
223-ZZ-C86	0.17	<28.	<4.0	1.3	0.04	(H) 0.12	—	43.	<100.	42.	180.	5.0

Table 1 -- continued

Field ID	Yb ppm ICP	Yb ppm NA	Zn ppm AA	Zn ppm ICP	Zn ppm NA	Zr ppm NA
223-A-C82	8.0	8.1	150.	150.	—	720.
223-D-C83	<1.00	0.47	—	27.	19.	110.
223-E-C83	10.	—	89.	<100.	—	—
223-F-C83	3.0	—	34.	30.	—	—
223-G-C83	12.	4.8	130.	110.	100.	—
223-P-C86	7.0	5.8	—	230.	310.	—
223-Q-C86	1.00	0.68	—	25.	40.	—
223-R-C86	<1.00	0.82	—	<4.0	83.	—
223-S-C86	9.0	5.3	—	150.	210.	<3300.
223-T-C86	<1.00	0.88	—	5.0	8.2	<82.
223-W-C86	6.0	3.0	—	70.	—	<1800.
223-W-C86R	8.0	5.8	—	61.	180.	<930.
223-Y-C86	<1.00	0.55	—	180.	30.	—
223-AA-C86	1.00	0.69	—	82.	93.	—
223-M1-C86	<1.00	0.15	—	270.	300.	<25.
223-N1-C86	1.00	0.95	—	35.	62.	—
223-N2-C86	9.0	7.8	—	150.	—	—
223-U1-C86	2.0	2.7	—	35.	55.	280.
223-U2-C86	2.0	2.6	—	50.	52.	270.
223-Z1-C86	2.0	1.9	—	36.	—	510.
223-ZZ-C86	<1.00	0.68	—	240.	260.	—

Ridenour orebody are depicted in figure 7, which shows, for most of the elements determined, their respective degrees of enrichment or depletion relative to unmineralized rock. Elements such as Ag, Co, Cu, Eu, Ni, Pb, U, and V are enriched more than 50 times background and Mo, Nd, Y, Yb, Zn, and most of the rare-earth elements are enriched more than 10 times background in more than half the samples analyzed from the Ridenour mine.

As a consequence of the severe erosion and oxidation of the mineralized rock from the Ridenour pipe, the original "pyrite cap" has been removed. This assumes that the Ridenour pipe contained a typical uranium breccia-pipe orebody with an overlying "pyrite cap"--there is no reason to believe otherwise based on the Ridenour structure, geochemistry, and oxidized mineral assemblage. The Fe and S from the eroded "pyrite cap", as well as from sulfides in the primary orebody, were apparently not remobilized during oxidation and carried downward in the pipe to the present mine level. Little sulfur remains in the rock; with the exception of two samples, which contain 4.7 and 0.5 percent sulfur, all of the samples have <0.1 percent sulfur. Likewise, the Fe enrichment of the Esplanade Sandstone in the pipe is minor compared to that shown by Wenrich (1985) for the unoxidized breccia pipes.

This oxidation of the Ridenour mine has apparently removed the primary uranium concentrations. At present, uranium enrichments generally occur within the ring fractures as hexavalent uranium minerals, which is in sharp contrast to the primary uraninite ore preserved in the unoxidized breccia pipes.

Several elements, notably Ag, Cu, and V, are distinctly enriched in the Ridenour pipe relative to Grand Canyon pipes that have been mined for uranium on the North Rim. These elements are discussed in more detail below. Oxidation of the Ridenour orebody appears to have played a major role in the concentration of these metals.

Metals Strongly Enriched at the Ridenour Pipe

Vanadium

The Ridenour orebody is exceptionally enriched in vanadium: 21 mineralized samples analyzed from the mine, all have vanadium concentrations exceeding 100 ppm, and 12 have concentrations >1% (table 1). The vanadium in all Ridenour samples is present in concentrations greater than that of uranium; the vanadium/uranium ratio averages about 4. Within most pipes on the Hualapai Reservation the greatest vanadium concentrations occur in the most oxidized samples. The average vanadium content of 83 unoxidized samples from North Rim orebodies, for example, is only 99 ppm (parts per million), and that of 25 unoxidized samples from South Rim orebodies is 162 ppm, in contrast to an average of 22,600 ppm (2.26%) for the Ridenour mine (fig. 8a). Vanadium/uranium ratios for the unoxidized ores generally are far less than 1, again in sharp contrast to the Ridenour mine. The only other known pipes with vanadium enrichment are the Orphan pipe, from which 3400 lb of V_2O_5 were produced (Chenoweth, 1986), and the Canyon pipe, from which 8 core samples averaged 311 ppm vanadium (7 of the 8 ranged between 190 and 670 ppm V; K.J. Wenrich, unpublished data, 1987). Both of these orebodies are on the South Rim and have contributed to the higher average vanadium content for South Rim ores in contrast to north rim ores (fig. 8a).

Vanadium in the Ridenour mine is represented chiefly by the minerals roscoelite--the vanadium mica--and volborthite, a copper vanadate. No primary vanadium minerals have yet been identified in unoxidized ores from Grand Canyon breccia pipes, and the mineralogic residence of this element remains

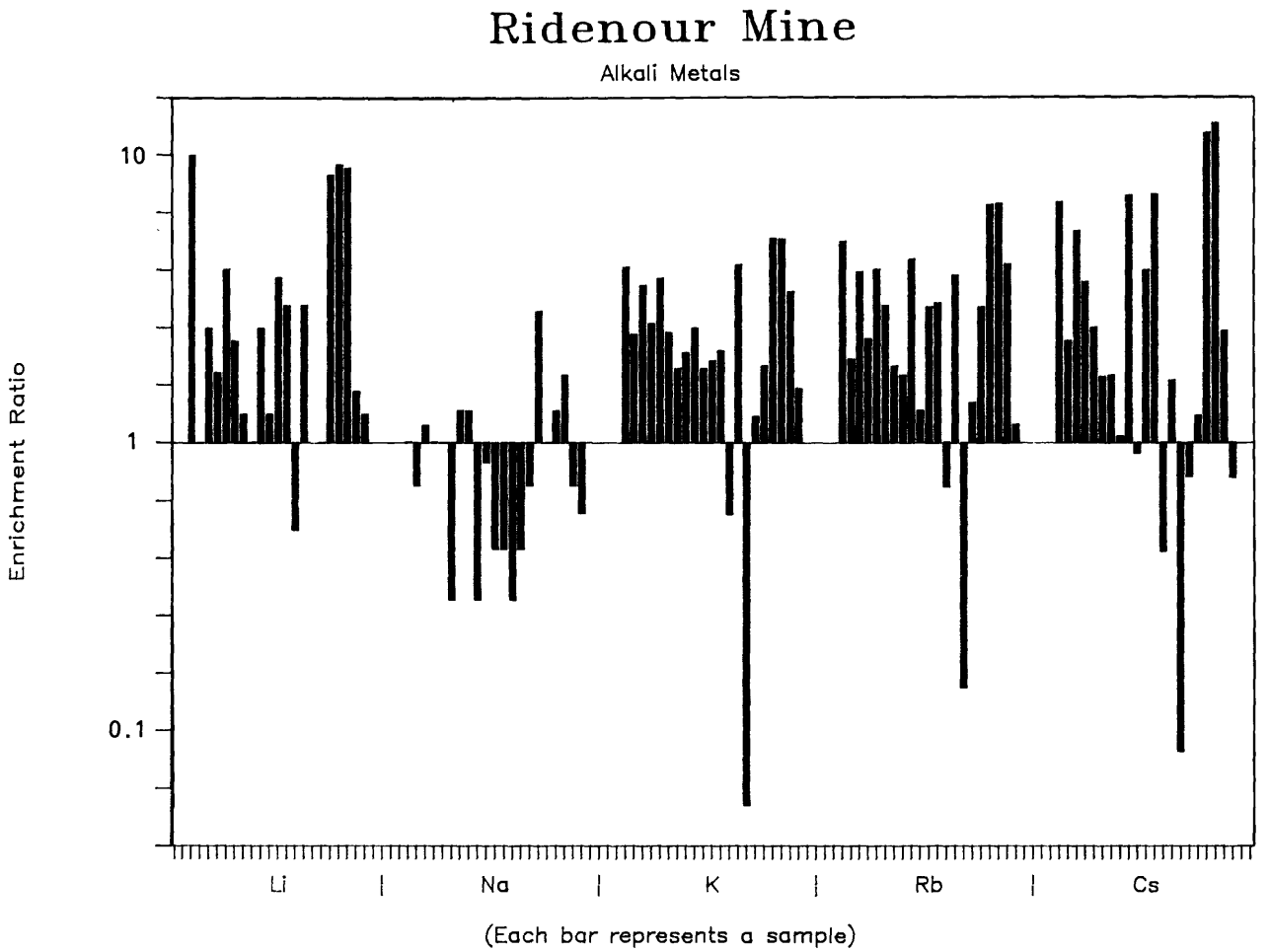

Figure 7. Enrichment ratios for each of the 21 samples collected at the Ridenour mine. The enrichment ratio for each element in each sample is the absolute concentration of that element in the mine sample divided by the average concentration of that element in background samples collected from the Esplanade Sandstone. These background values were compiled from an average of 4 unaltered, unmineralized, Esplanade Sandstone samples collected from 4 regionally separate locations that are not near any known breccia pipes. Each bar on this figure represents a separate sample; blank spaces mean no data (or only a "less than value") was available for that sample. This then indicates whether an element was enriched or depleted 10, 100, 1000, etc. times the background value. Samples are arranged from left to right for each element in the order that they are shown in table 1.

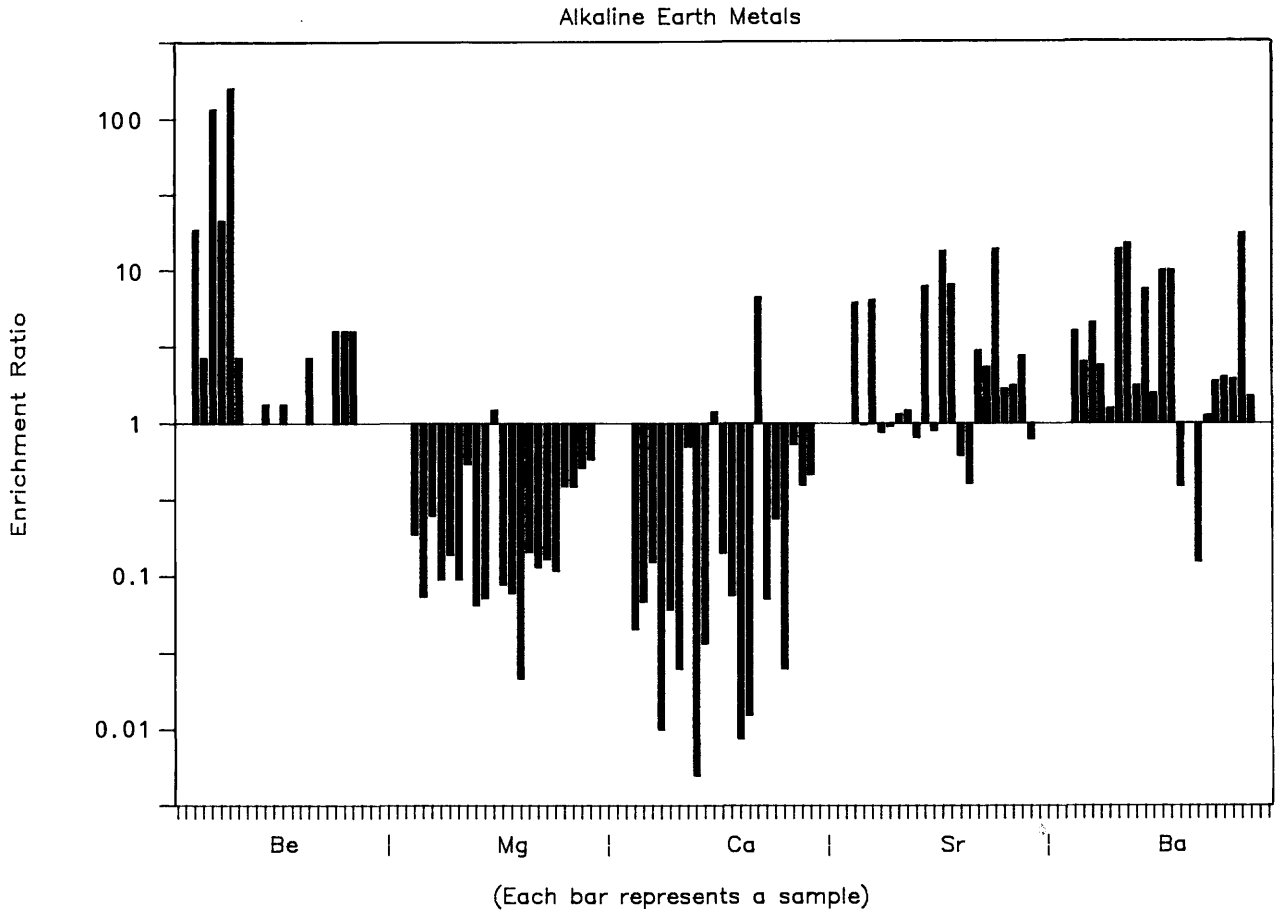

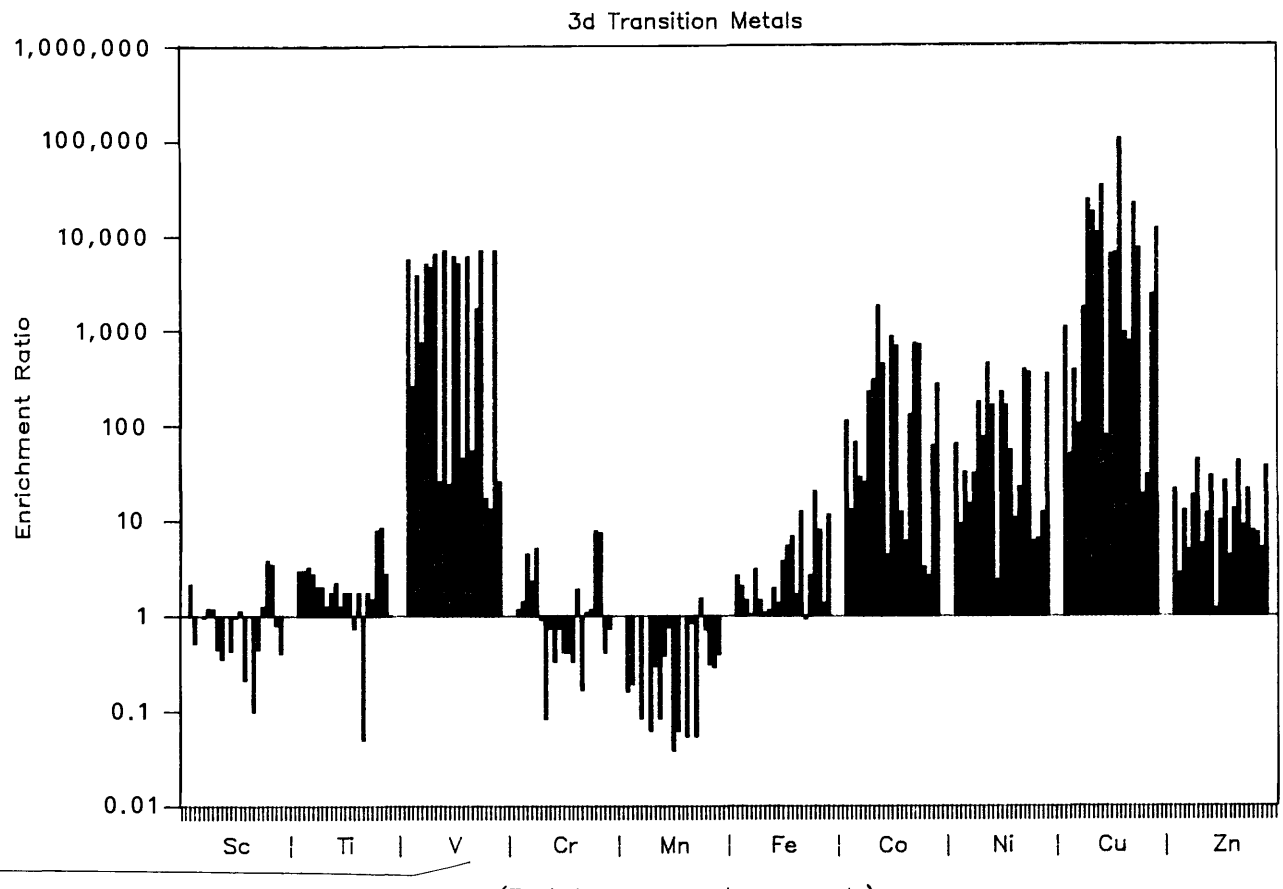

Figure 7. Continued.

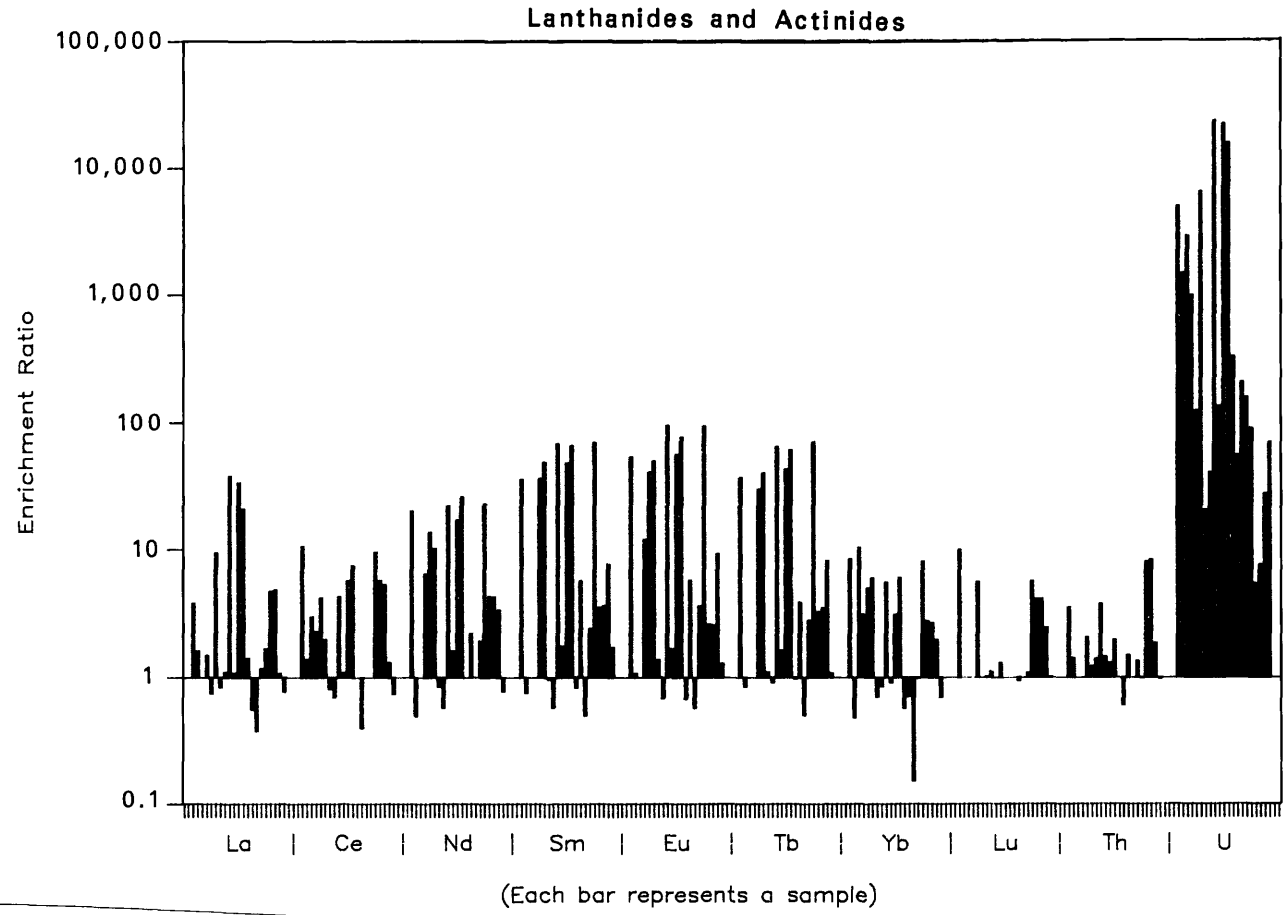

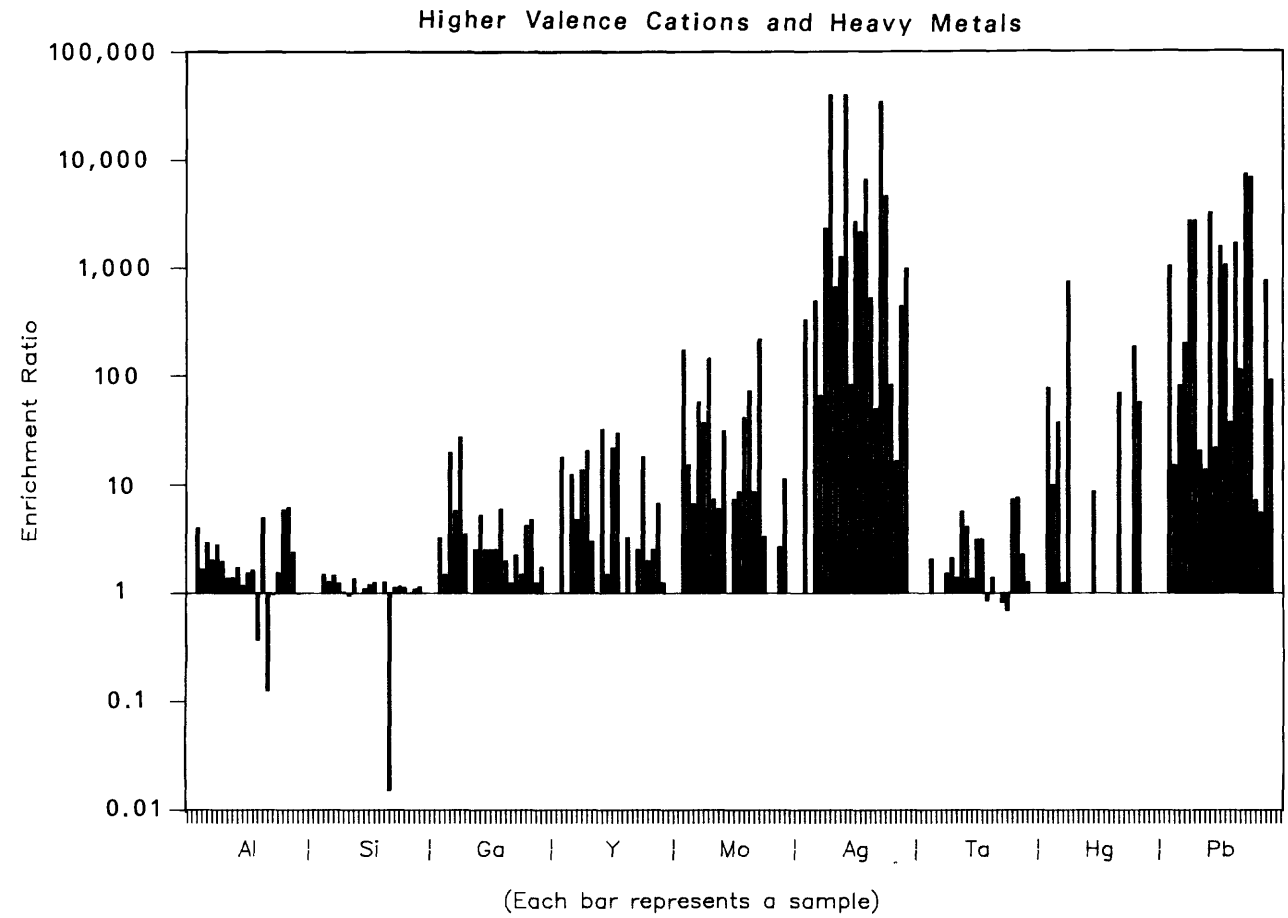

Figure 7. Continued.

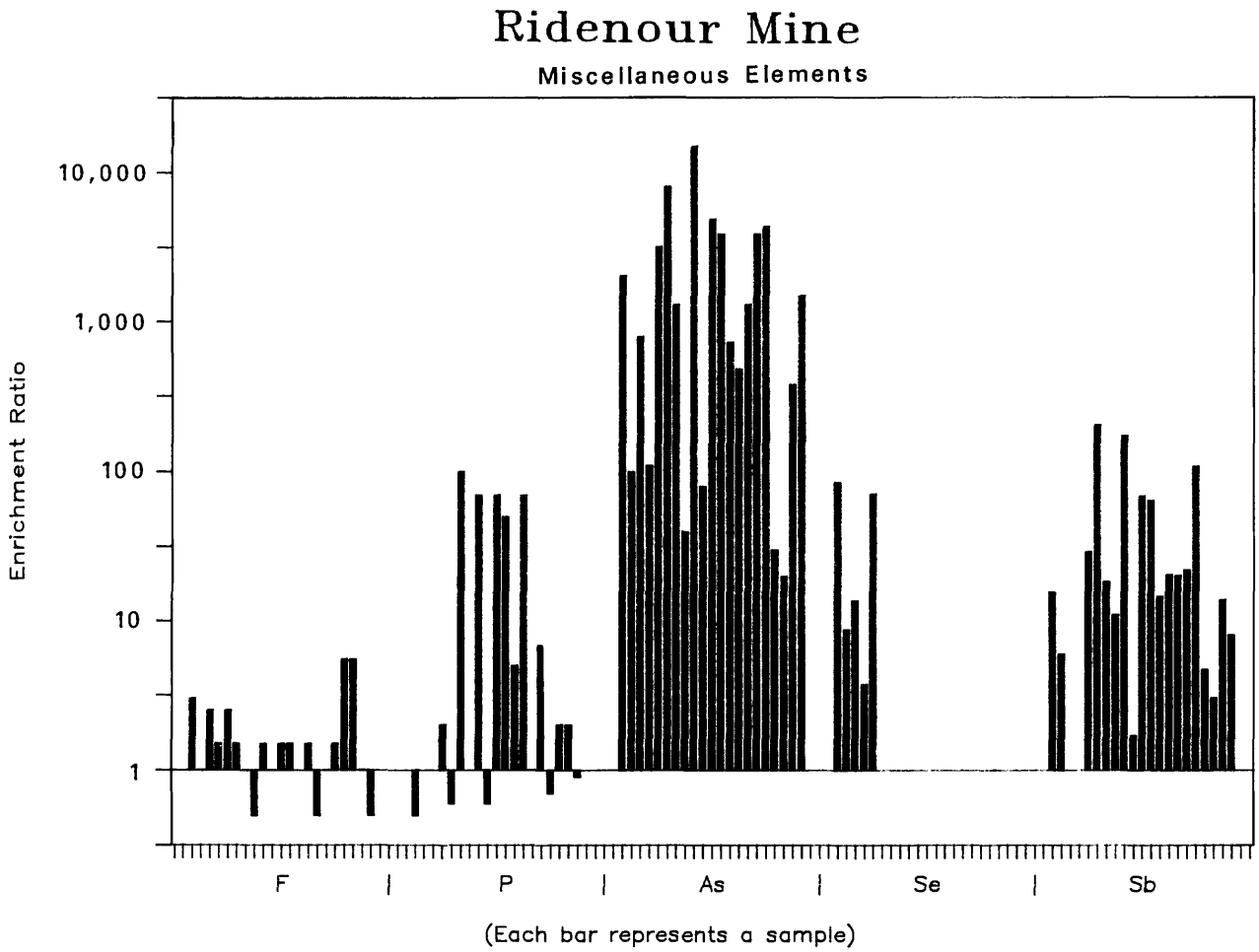

Figure 7. Continued.

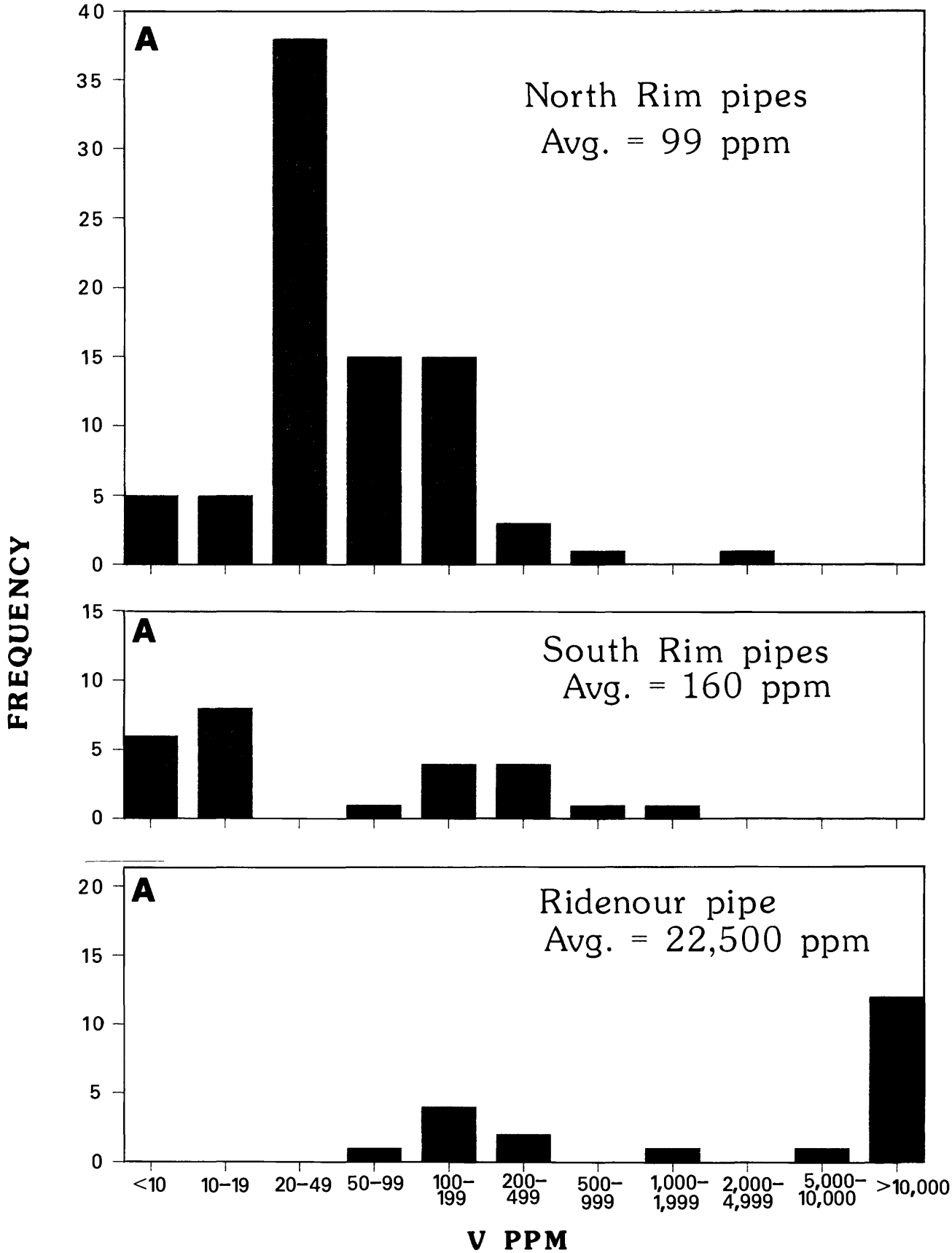

Figure 8. Frequency histograms for vanadium (A) and silver (B) concentrations comparing 83 unoxidized samples from 11 uranium breccia pipe orebodies on the North Rim of the Grand Canyon with 25 unoxidized samples from 3 uranium breccia pipe orebodies on the South Rim. Histogram intervals are log scales.

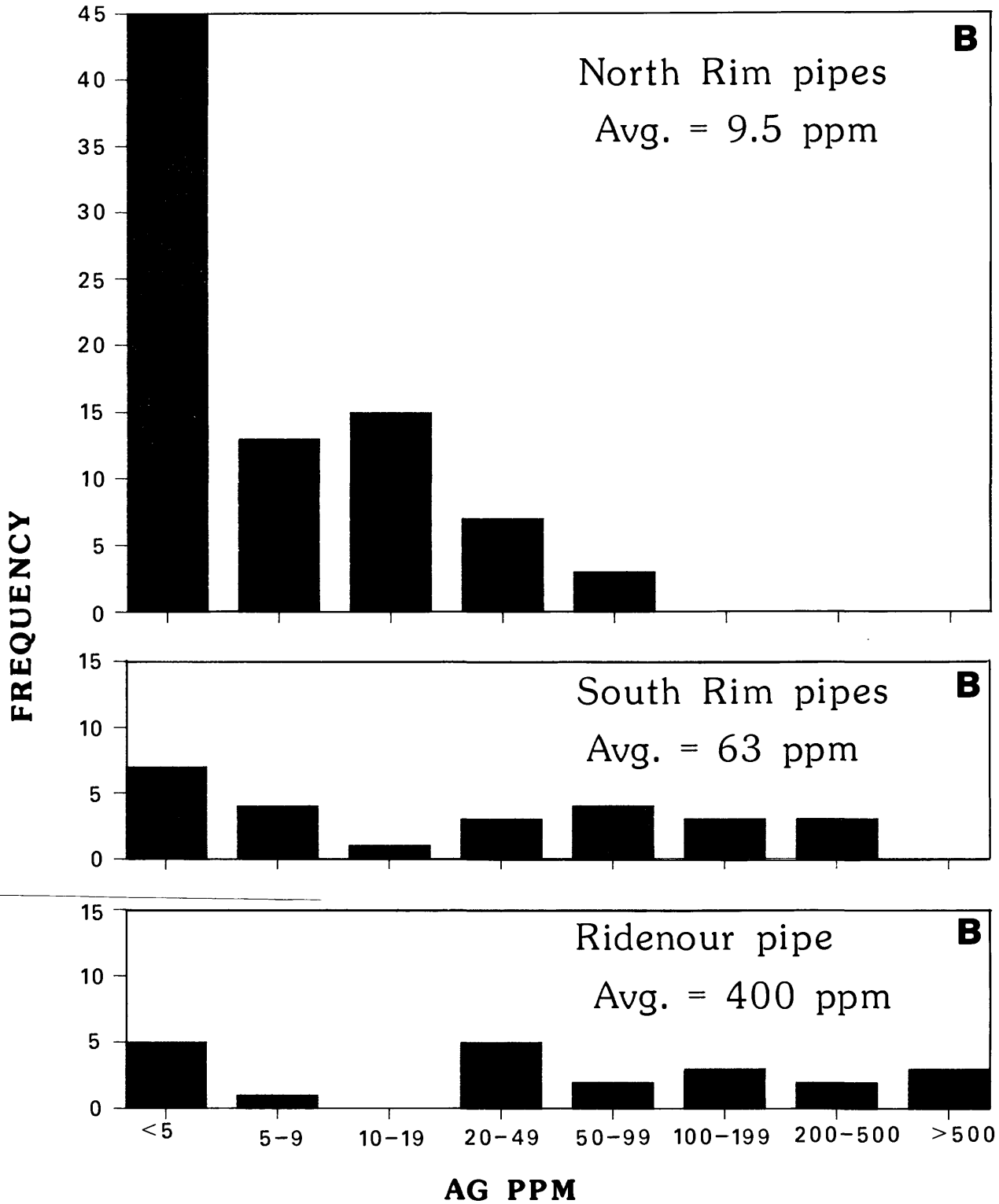

Figure 8. Continued.

largely unknown. For similar reasons the manner in which vanadium was deposited as a trace constituent of the primary ores, later to become concentrated upon oxidation, remains ill-defined.

Silver

Silver, like vanadium, is highly enriched in the oxidized ores of the Ridenour mine. Concentrations of silver in three samples exceed 2000 ppm (table 1), more than double the silver content of any of the 383 samples (both surface and subsurface) collected from other breccia pipes throughout northwestern Arizona (K.J. Wenrich and H.B. Sutphin, unpublished data, samples collected 1979-1989). The average silver content of 21 Ridenour samples is 400 ppm, far exceeding the average of 10 ppm for 83 unoxidized samples from uranium orebodies in North Rim pipes and the average of 63 ppm for 25 unoxidized samples from uranium orebodies in South Rim pipes (fig. 8b).

Copper

The Ridenour mine, like most pre-1980 mines in the Grand Canyon area, was originally developed for its copper ore. Copper in the Arizona breccia pipes behaves similarly to silver and vanadium, in that it is more concentrated in South Rim pipes than North Rim pipes. For the 21 samples collected from the Ridenour mine the average copper concentration is 6% (60,000 ppm), which compares well to the 5.8% (58,000 ppm) average for 25 unoxidized samples from other South Rim orebodies, but is significantly higher than the 3700 ppm average for 83 unoxidized samples from North Rim orebodies (K.J. Wenrich, unpublished data).

Gallium

Gallium is the only other element whose enrichment in the Ridenour pipe notably exceeds that of most other Grand Canyon pipes. Two of the Ridenour samples contain concentrations of 80 and 110 ppm, more than any of the other 383 breccia pipe samples that have been analyzed (K.J. Wenrich, unpublished data). The gallium content of most breccia pipe samples is <20 ppm; only 6 unoxidized samples of the 108 collected from breccia pipe orebodies contain gallium concentrations in excess of 20 ppm and the maximum of these 6 is 69 ppm gallium. However, even the most gallium-rich samples from the Ridenour mine, 80 and 110 ppm, represent only a third of the average concentration determined in samples collected from the Apex mine breccia pipe farther west, in the Basin and Range province in southwestern Utah (near St. George). Hecla Corporation is preparing to recover gallium and germanium from the Apex pipe. The Apex orebody, like that of the Ridenour mine, is an oxidized solution-collapse breccia pipe that probably bottoms in the Redwall Limestone (Wenrich and others, 1987); it too was originally developed for its copper ore. Of 22 jarosite- and goethite-rich samples collected from the Apex pipe, gallium concentrations range from 38-1400 ppm and average 283 ppm (K.J. Wenrich, unpublished data). The enrichment of gallium at both the Ridenour and the Apex mines, is a probable consequence of the strong oxidation of these orebodies.

Isotopic Studies

Whole-rock quartz $\delta^{18}O$ values from the Esplanade Sandstone show virtually no difference between the background sample and the three mineralized samples (table 2). Apparently the isotopic composition of the detrital quartz in the sandstone remained unaffected by later mineralizing fluids despite the evident

Table 2--Isotopic composition of Ridenour mine samples. Sample locations are shown on figure 6. The Esplanade Sandstone background sample (PE-A-C83) was collected 2 miles from the mine along the road descending from the Coconino Plateau. (--- = not determined)

	223-B-C83	223-E-C83	223-G-C83	PE-A-C83 Background
$\delta^{13}C$(PDB) carbonate	---	---	-1.7	1.7
$\delta^{18}O$(PDB) carbonate	---	---	-7.9	-3.2
$\delta^{18}O$(SMOW) quartz	12.6	12.2	13.0	12.8
$\delta^{18}O$(SMOW) clay	12.4	---	---	---
*$^{206}Pb/^{204}Pb$ whole rock	22.04	---	---	---
*$^{207}Pb/^{204}Pb$ whole rock	15.88	---	---	---
*$^{208}Pb/^{204}Pb$ Whole rock	39.38	---	---	---

*Analyses by K.R. Simmons, U.S. Geological Survey, Denver, Co. 80225; sample contained 76 ppm uranium and 9400 ppm lead.

corrosion of quartz grains in some of the samples examined (Appendix B). In contrast, $\delta^{18}O$ values in the carbonate fraction from mineralized rock are less than that for the background Esplanade Sandstone carbonate (table 2). Two possible explanations for the observed data are: (1) the mineralizing fluids from which carbonate minerals precipitated within the Ridenour breccia pipe were warmer than the fluids that deposited the original carbonate cement in the host Esplanade Sandstone, or (2) the mineralizing fluids had a lower initial $\delta^{18}O$ composition (more meteoric). Fluid inclusion studies of primary ore-zone dolomite and carbonate (from other breccia pipe mines in northwestern Arizona) yield dolomite primary fluid inclusion salinities from these ore-bearing pipes of >17 wt % NaCl eq., and temperatures in the range of 105°-161°C (James Reynolds, written communications, 1984-1990). Hence, the mineralizing fluids that lowered the original Esplanade Sandstone carbonate $\delta^{18}O$ values and created lower carbonate $\delta^{18}O$ values within the mineralized zone were probably warm brines. Neither scenario above can be eliminated by confirmation that the mineralizing fluids were warm brines; warm brines agree well with the first scenario, and the second scenario simply indicates that the brines could not have been marine in origin, but rather must have been from meteoric water that may have come in contact with rock rich in salts.

Carbon isotopic compositions of carbonate also differ between mineralized and background samples of Esplanade Sandstone (table 2). The more negative $\delta^{13}C$ values in the mineralized rock probably reflect the presence of organic compounds in the mineralizing fluids; evidence for this can be found in the association of bitumen with uranium ore in a few breccia pipes and the occurrence of organic material within some sphalerite fluid inclusions (Wenrich and Sutphin, 1989).

The Pb-whole rock isotopic ratios (table 2) plot in the same Pb isotopic field as the ratios for some of the most-radiogenic galenas collected from pipes with economic concentrations of uranium (K.R. Ludwig, personal communication, 1989). This similarity suggests that even though the Ridenour breccia pipe no longer contains economic concentrations of uranium, the pipe may have before it was oxidized and severely dissected.

MINERALOGY

The collapse breccia contained within the breccia pipes was an excellent, highly porous host for mineral deposition. The unaltered pipe material consists of clasts, which vary in size from 0.1 in to over 30 ft, derived from overlying units, primarily carbonate- or silica-cemented sandstones and siltstones. The breccia matrix is composed of individual sedimentary framework grains that were decemented and freed from their host formations during and following collapse. High porosity is characteristic of the space between the individual matrix framework grains, which are >95% quartz. Vugs not filled by breccia matrix commonly became host sites for deposition of coarsely crystalline calcite, barite, and gypsum.

Strong zoning within the breccia pipe orebodies appears uncommon; most minerals are somewhat irregularly distributed throughout most of the orebody. The major exception to this is the development of a "pyrite cap" over the uranium orebody that for the most part consists of pyrite-impregnated sandstone grading to massive pyrite with few associated ore minerals (except for related cubic Ni-Co-Fe-bearing sulfides, such as bravoite, and arsenides, such as gersdorffite). In some pipes, such as the Orphan and Ridenour, uranium ore has accumulated in an annular zone around as well as within the pipe, but in most of the other mines the uraninite is concentrated within the

pipe. The highest-grade uranium appears to be well below the "pyrite cap" toward the center of the orebody.

The mineralogy of the breccia-pipe orebodies is remarkably similar from pipe to pipe, although minor variation is present between pipes north and south of the Grand Canyon. The ore horizon appears to be slightly lower south of the Grand Canyon--commonly at the level of the Esplanade Sandstone--whereas to the north most ore is located at the Hermit Shale horizon. The mineral paragenesis is fairly consistent from pipe to pipe (earliest to latest): (1) quartz, calcite, dolomite, barite, siderite, kaolinite; (2) Ni-Co-As-Fe sulfides and arsenides, such as siegenite, bravoite, pyrite, millerite, gersdorffite, rammelsbergite, niccolite, arsenopyrite, and marcasite; (3) Cu-Fe-Zn-Pb sulfides such as chalcopyrite, enargite, galena, sphalerite, pyrite and uraninite; (4) supergene alteration minerals, such as malachite, azurite, cyanotrichite, and brochantite (Wenrich and Sutphin, 1989). In addition to the above minerals, pipes on the South Rim (the Orphan, Canyon, and Ridenour pipes) contain copper sulfides, such as bornite, chalcocite, djurleite, digenite, and covellite that form under slightly higher Eh conditions than do chalcopyrite and enargite (Garrels and Christ, 1965). These higher-Eh copper sulfides generally are later in the paragenetic sequence than uraninite.

Oxidation at the Ridenour pipe has been sufficiently extensive that primary ore minerals, such as uraninite, pyrite, chalcopyrite, bravoite, siegenite, arsenopyrite, galena, and sphalerite that are common in unaltered breccia pipe orebodies, have been almost totally removed. Of these minerals, only trace amounts of pyrite and galena have been observed within samples from the Ridenour mine. Even the large goethite concretions or pseudomorphs of limonite after pyrite that are so common in the oxidized zones of some other pipes are almost totally absent from the Ridenour pipe. Few opaque minerals remain; those seen are only highly corroded remnants. Those minerals present are almost exclusively of secondary origin and many are clearly supergene, deposited as fracture fillings, and as replacements of sandstone or breccia matrix, which encases abundant disaggregated quartz grains. In the ring-fracture breccia nearly all mineralization was confined to the matrix with only minor "bleeding" of malachite and other secondary minerals into the clast margins. Minerals such as chalcocite and digenite in some samples are present in concentrations of more than 1 percent, and although they represent some of the few sulfides remaining, they themselves may be oxidation products of the primary minerals chalcopyrite and enargite. Appendix B provides detailed petrographic descriptions of the samples collected from the locations shown in figure 6.

The 1-5 percent vanadium commonly present in mineralized rock at the Ridenour mine occurs primarily in volborthite (fig. 9, see also Appendix C for microprobe analyses) and roscoelite (fig. 10b), and less commonly as vesignieite and calciovolborthite. The roscoelite and volborthite, like nearly all the other secondary minerals, replace the matrix carbonate (fig. 10a), composed originally of calcite and dolomite. Uranium has been found only in the hexavalent oxidation state, as tyuyamunite and metatyuyamunite, filling the ring fractures and replacing the carbonate matrix of the host sandstone and breccia. Although both Miller (1954) and Chenoweth (1988) reported carnotite at the Ridenour mine, X-ray diffraction patterns of numerous yellow radioactive fracture encrustations from throughout the mine failed to confirm its presence.

Most minerals at the Ridenour are extremely fine-grained and disseminated through the breccia and sandstone matrices, and cannot be identified without scanning electron microscope or electron microprobe analyses. Although the 21

Figure 9. Transmitted light photomicrograph of volborthite ($Cu_3(VO_4)_2 \cdot 3H_2O$) crystals (yellow in transmitted light) surrounded by calcite (clear). Width of field is 0.25 mm. Sample 223-Q-C86.

A.

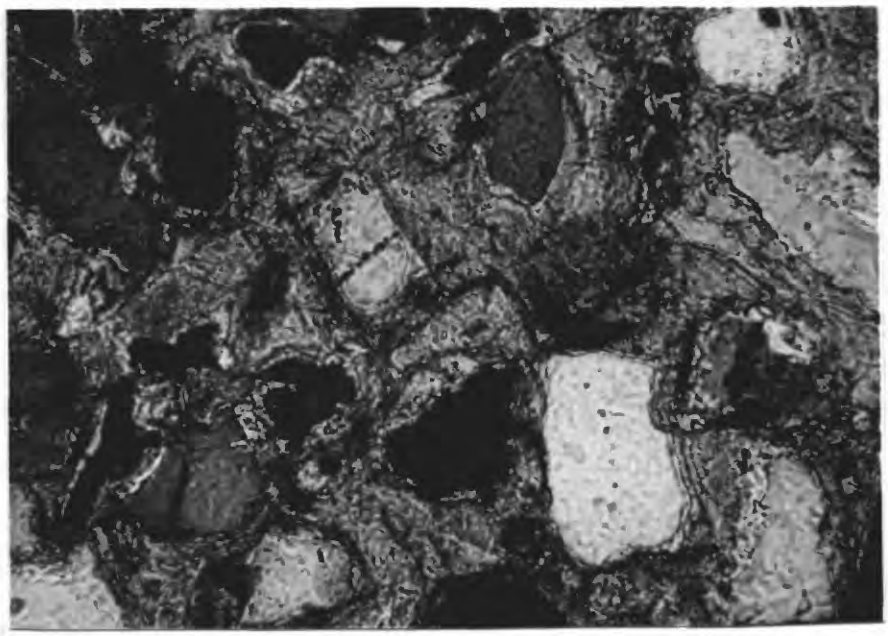

B.

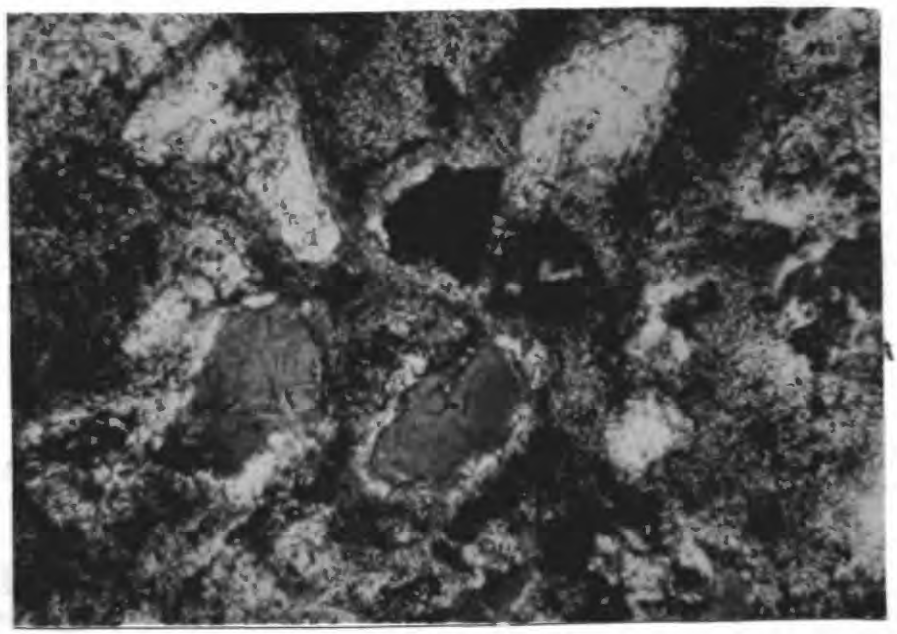

Figure 10. **A.** Esplanade Sandstone from the mine (sample 223-G-C83) with recrystallized dolomite cement between the detrital quartz grains. The horizontal field of view is 0.52 mm. **B.** Esplanade Sandstone from the same stratigraphic horizon (sample 223-A-C83), but mineralized with 4% vanadium. In this sample the dolomite cement has been replaced by roscoelite, $K(V,Al,Mg)_2AlSi_3O_{10}(OH)_2$. Long dimension of photo is 0.45 mm.

samples collected from the Ridenour mine have an average silver concentration of 400 ppm, identification of silver-bearing minerals has been difficult. The only silver minerals identified to date are naumannite (fig. 11) and acanthite.

An unidentified Cu-V arsenate forms pale green transparent hexagons (in thin section) adjacent to highly corroded detrital quartz grains. The mineral contains Cu and As in about a 2.75:1 ratio, and it also contains about 5 wt percent V_2O_5. In addition, an unidentified cobalt oxide forms a black fracture coating. Appendix C lists microprobe analyses for the cobalt oxide, the Cu-V arsenate, and cavity-filling calcite.

The paragenetic sequence for the Ridenour mine is shown in figure 12. Pyrite and galena are obviously two of the earliest phases as they are essentially the only remnants of the primary orebody. Two stages of barite are present: (1) an earlier barite represented by empty crystal molds, and (2) a late stage golden barite deposited on fracture surfaces with volborthite.

DISCUSSION OF RIDENOUR PIPE MINERALIZATION

The collapse breccia contained within the breccia pipes was an excellent, highly porous host for mineral deposition. Nevertheless, once the pipes were mineralized by uraninite, Cu-Pb-Zn minerals, and the "pyrite cap", the orebodies appear to have been little altered by fluid movement until the Pliocene, when the present period of canyon dissection probably began in northwestern Arizona. Most pipes lying directly within the Grand Canyon and its tributaries have been oxidized to some degree by downward-moving groundwater. Pipes that have been dissected below the level of the "pyrite cap", such as the Ridenour, generally have little or no primary ore remaining--that is, what uranium remains in the rock is present only as hexavalent uranium minerals, and uraninite is rarely preserved.

Geochemical data for 383 mineralized breccia pipe samples (K.J. Wenrich, unpublished data), both oxidized and unoxidized, suggest that two independent processes--the degree of secondary oxidation of the ores and perhaps also the Eh-pH of the ore-forming fluids--dramatically affected ore compositions. Silver, vanadium, and gallium are among those elements clearly enriched in oxidized supergene ores. The oxidized Ridenour ores furnish one extreme example, but there are many others: oxidized surface samples collected from old copper prospects in other pipes commonly contain more than 150 ppm each of silver and vanadium, far more than their unoxidized equivalents in subsurface mines presently being exploited for uranium. Conversely, oxidized ores generally contain far less uranium, which under supergene conditions is readily leached from permeable rocks and removed in solution. The Ridenour mine was first and foremost a copper mine and produced only small tonnages of uranium ore from scattered and highly localized parts of the orebody.

The effect of mineralizing-fluid Eh on ore composition is less readily documented, but may have been a contributing factor to the relatively high silver content of the Ridenour orebody. The suggestion rests on a series of observations tied to a geochemical argument:

(1) Silver is present in some of the mineralized samples examined during the Ridenour mine study as the minerals acanthite (Ag_2S) and naumannite (Ag_2Se); in the primary ores on the North Rim, however, microprobe X-ray maps have shown that the little silver that is present resides in copper sulfides, presumably tennantite or enargite;

A.

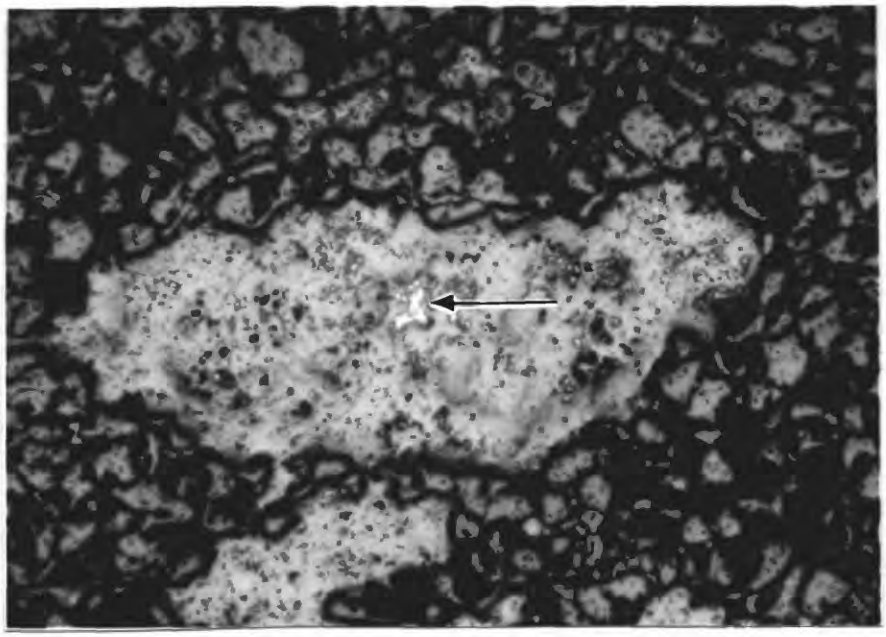

B.

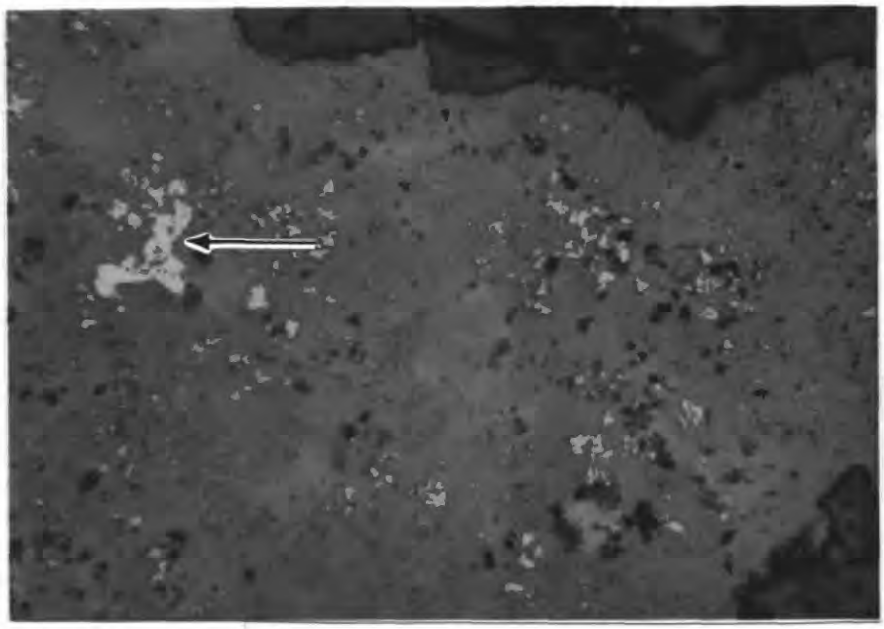

Figure 11. **A.** Reflected-light photomicrograph of malachite-impregnated Esplanade Sandstone containing 2100 ppm Ag (sample 223-N1-C86). Detrital quartz grains are surrounded by a matrix containing tyuyamunite and roscoelite. Long dimension of photo is 1.7 mm. **B.** Blow-up of the center of photograph **A**--arrows in each photo point to the same grain of naumannite. Note the small, highly reflective areas of naumannite (Ag_2Se) and acanthite (Ag_2S). Long dimension of photo is 0.68 mm.

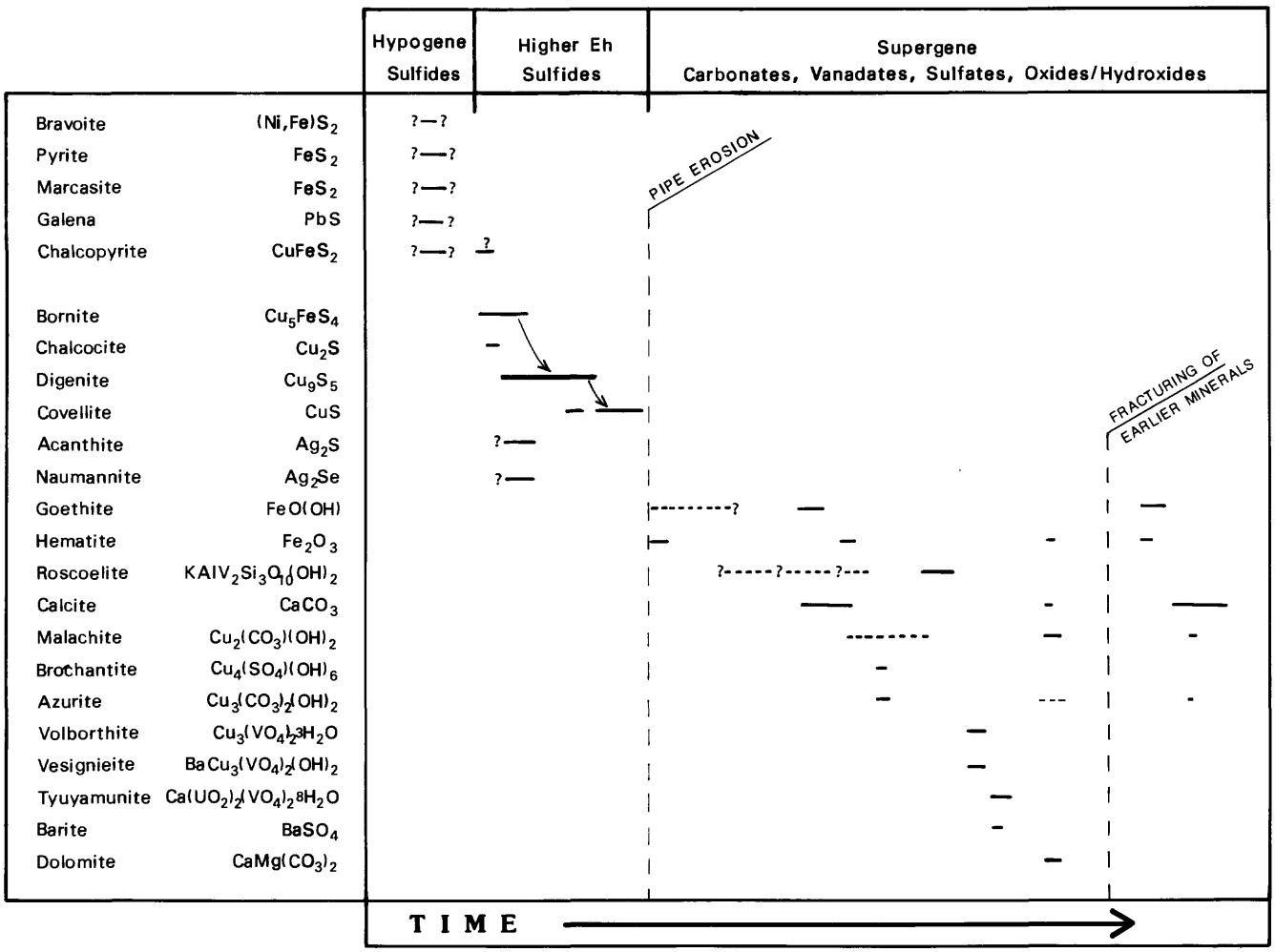

Additional Minerals Present

Calciovolborthite	$CaCu(VO_4)(OH)$	Illite		Metatyuyamunite	$Ca(UO_2)(VO_4)_2 \cdot 5(H_2O)$
Conichalcite	$CaCu(AsO_4)(OH)$	Kaolinite		Siderite	$FeCO_3$
Cuprite	Cu_2O	Limonite		Tenorite	CuO

Figure 12. Paragenetic sequence for minerals found at the Ridenour mine. Arrows indicate alteration of one mineral to the next, such as digenite altered to covellite.

(2) The Eh-pH stability field of Ag_2S largely overlaps that of such copper sulfides as chalcocite and covellite (Brookins, 1988) so that simultaneous precipitation of acanthite (and presumably, because it occurs with acanthite, the selenide naumannite as well) with these sulfide minerals is geochemically reasonable;

(3) The above-mentioned sulfides are most common in South Rim orebodies, where the assemblage chalcopyrite-chalcocite-djurleite-digenite-covellite-bornite appears characteristic (Wenrich and others, 1988);

(4) North Rim ores, in contrast, contain little chalcocite, covellite or any of the above mentioned assemblage except chalcopyrite, but instead contain the minerals chalcopyrite, tennantite, and enargite, which are stable under lower Eh conditions (Wenrich and others, 1988).

From these relations (specifically the favorable Eh-pH conditions at the Ridenour pipe for the precipitation of at least one sulfide with essential silver), one might expect larger quantities of silver minerals to have been deposited in the South Rim ores, a conclusion consistent with the average silver contents of unoxidized ores shown in figure 8b. The difference in silver content between North and South Rim orebodies, then, may be due not so much to differences in composition of the mineralizing fluids but rather to differences in Eh-pH conditions during sulfide precipitation, with higher Eh conditions prevailing toward the south. The subsequent oxidation of the orebody apparently concentrated the silver above levels that are normally found in South Rim unoxidized orebodies (fig. 8b).

The presence of the relatively rare vanadium mica, roscoelite, at the Ridenour mine represents its first reported occurrence in the breccia pipes. Roscoelite contains trivalent vanadium, indicating that the conditions under which it was precipitated could not have been strongly oxidizing. Whether the roscoelite was part of the primary ore has not been conclusively determined, although its seeming absence from any of the primary orebodies suggests that it may have been secondary. Nevertheless, its fine-grained nature in the Ridenour pipe renders it difficult to identify, and so it may be present, but unrecognized in other Arizona pipes, specifically the South Rim pipes. Roscoelite occurs at the Ridenour in the ring fracture zone in association with hexavalent uranium minerals and malachite. Roscoelite is very stable once it has formed, such that subsequent oxidation would probably not have destroyed it (G.N. Breit, personal communication, 1990). Hence, the roscoelite could have formed at any time during mineralization of the Ridenour pipe, although its absence from the primary orebodies suggests that it was later than the U-Cu-Pb-Zn mineralization phases.

Acanthite, chalcocite and covellite were formed in an acid environment under moderately oxidizing conditions (Brookins, 1988) at the Ridenour pipe; these minerals postdate deposition of bravoite, pyrite, marcasite, galena, and chalcopyrite. Because both chalcocite and covellite also occur at the Orphan mine and are there associated with late-stage uraninite, it is assumed here that they formed prior to conditions that were sufficiently oxidizing to destroy uraninite--that is, prior to dissection of the pipe and precipitation of supergene minerals such as malachite and azurite. The Ridenour pipe has a conspicuous absence of sulfur and iron (table 1)--there is little gossan development and compared to most pipes within the Canyon little limonite or hematite in outcrop. Presumably, during the past 5.5 m.y. when Grand Canyon dissection became intensive (Lucchitta, 1987), the ores at the Ridenour mine were sufficiently oxidized, perhaps at a low pH, so that most sulfur and iron from the primary minerals were removed.

DRILLING

Three vertical holes were drilled into the Ridenour pipe during 1976 by Western Nuclear, Inc. to depths of 324 ft, 440 ft, and 990 ft (data from the Hualapai Tribal office files) at the locations shown on fig. 1. The two shallower holes were collared along the road that parallels, and lies just east of, the western part of the ring-fracture zone (fig. 6). These two holes began within the pipe. The deeper hole to 990 ft was placed outside the ring fracture zone, slightly to the west of the pipe. The gamma radiation never exceeded 40 cps in any of the three holes, and apparently little of the rock encountered was mineralized or reduced. The only signs of any mineralized rock were located between a depth of 715 ft and 990 ft, which should be within the Watahomigi Formation and Redwall Limestone, respectively, where traces of pyrite were observed. The lease was dropped in 1978, apparently because the property was believed to have little economic potential and had poor access.

If the property is ever drilled in the future, holes should be placed toward the center of the pipe, either near the bottom of the drainage, or along the road as angle holes inward to the core of the pipe. All previous holes were vertical and apparently did not go into the center of the pipe.

ECONOMIC POTENTIAL OF THE RIDENOUR MINE

The Ridenour mine resembles an oxidized version of the Orphan breccia pipe, which is located just below Grand Canyon Village at the base of the Coconino Sandstone cliff. The geochemistry and the stratigraphic and structural control of most ore within the ring-fracture zone of the Esplanade Sandstone are identical in both pipes. The Orphan mine produced 4.26 million lb of U_3O_8 from 1959-1969 (Chenoweth, 1986). Nearly all production from the Orphan mine came from the Esplanade Sandstone, the same as at the Ridenour mine. The Wescogame Formation also contained some ore at the Orphan mine, but the amount was minor compared to that produced from the Esplanade. At the Ridenour mine the Esplanade ore has been almost completely oxidized, and the center of the pipe at this stratigraphic level has been almost totally removed by erosion. If the Ridenour pipe is similar to the Orphan, then perhaps little ore is to be found in the underlying Wescogame or Manakacha Formations; nevertheless, both are primarily sandstones and, on that basis, should have been favorable hosts for mineralization. The center of the Ridenour pipe is preserved under the dump and in the bottom of the drainage below and within the lower part of the Wescogame Formation. Any future exploration should be restricted to these horizons.

The oxidation of breccia pipes such as the Ridenour pipe removed the uranium and concentrated elements such as copper, vanadium, and silver. Production records for breccia-pipe mines in the Grand Canyon during the last 100 years show that many of the mines produced silver, almost solely from oxidized copper ore, such as was found at the Ridenour mine. The high-grade vanadium probably has the greatest potential of any metal at the Ridenour mine for ore production, although the difficulty of access to the mine may preclude any future mining without significant increases in the price of metals.

ACKNOWLEDGEMENTS

The authors wish to thank George Billingsley for his geological insights and advice, and William Thoen for his computer compilation and graphical presentations of the geochemical data. Mitchell Henry assisted in the oxygen- and carbon-isotope interpretations. K.R. Simmons performed the lead isotopic analyses and K.R. Ludwig explained their significance to us--their published isotopic work on the uranium-lead ages (Ludwig and Simmons, 1988) has contributed significantly to our understanding of the mineralizing events that produced the uranium orebodies. Chemical analyses shown in table 1 were completed by David Fay, Ardith Bartel, Carol Gent, Brooke Hatfield, John Sharkey, Edith Engleman, Larry Jackson, Bruce Vaughn, David McKown, and James Budahn. Thanks to K.R. Ludwig for taking the time to look over the manuscript and providing suggestions for improving it. Appreciation also goes to the Hualapai Tribe for permission to publish the results of the 1976 Western Nuclear drilling at the Ridenour mine. This project was funded by the Bureau of Indian Affairs in cooperation with the Hualapai Tribe.

REFERENCES CITED

Aruscavage, P.J., and Crock, J.G., 1987, Atomic absoption methods, in Baedecker, P.A., ed., Methods for geochemical analysis: U.S. Geological Survey Bulletin 1770, p. C1-C6.

Baedecker, P.A. and McKown, D.M., 1987, Instrumental neutron activation analyses of geochemical samples, in Baedecker, P.A., ed., Methods for geochemical analysis: U.S. Geological Survey Bulletin 1770, p. H1-H14.

Billingsley, G.H., 1986, Relations of the Surprise Canyon and Watahomigi Formations to breccia pipes in the Grand Canyon, Arizona: Geological Society of America Abstracts with Programs, v. 18, no. 5, p. 342.

Billingsley, G.H., Wenrich, K.J., and Huntoon, P.W., 1986, Breccia pipe and geologic map of the southeastern Hualapai Indian Reservation and vicinity, Arizona: U.S. Geological Survey Open-File Report 86-458-B, 26 p., 2 plates, scale 1:48,000.

Brookins, D.G., 1988, Eh-pH diagrams for geochemistry: Springer-Verlag, New York, 176 p.

Chenoweth, W.L., 1986, The Orphan Lode mine, Grand Canyon, Arizona, a case history of a mineralized, collapse-breccia pipe: U.S. Geological Survey Open-File Report 86-510, 126 p.

_____1988, The production history and geology of the Hacks, Ridenour, Riverview and Chapel breccia pipes, northwestern Arizona: U.S. Geological Survey Open-File Report 88-0648, 60 p.

Damon, P.E., 1968, Correlation and chronology of ore deposits and volcanic rocks: Annual Progress Report no. COD-689-100, Research Division, U.S. Atomic Energy Commission, p. 49-50.

Garrels, R.M. and Christ, C.L., 1965, Solutions, Minerals, and Equilibria: San Francisco, CA, Freeman, Cooper and Company, 450 p.

Huntoon, P.W., 1970, The hydromechanics of the groundwater system in the southern portion of the Colorado Plateau, Arizona: Tucson, Ariz., University of Arizona Ph.D. dissertation, 251 p.

Huntoon, P.W., and Sears, J.W., 1975, Bright Angel and Eminence faults, eastern Grand Canyon, Arizona: Geological Society of America Bulletin, v. 86, p. 465-472.

Jackson, L.L., Brown, F.W., and Neil, S.T., 1987, Major and minor elements requiring individual determination, classical whole rock analysis, and rapid rock analysis, in Baedecker, P.A., ed., Methods for geochemical analysis: U.S. Geological Survey Bulletin 1770, p. G1-G23.

Lichte F.E., Golightly, D.W., and Lamothe, P.J., 1987, Inductively coupled plasma-atomic emission spectrometry, in Baedecker, P.A., ed., Methods for geochemical analysis: U.S. Geological Survey Bulletin 1770, p. B1-B10.

Lucchitta, Ivo, 1987, The mouth of the Grand Canyon and edge of the Colorado Plateau in the Upper Lake Mead area, Arizona, in Beus, S.S., ed., Centennial Field Guide Volume 2: Rocky Mountain Section of the Geological Society of America, p. 365-370.

Ludwig, K.R., and Simmons, K.R., 1988, Progress in U/Pb isotope studies of collapse-breccia pipes in the Grand Canyon region, northern Arizona: Geological Society of America Abstracts with Programs, v. 20, no. 7, p. A139.

McKee, E.D., 1982, The Supai Group of the Grand Canyon: U.S. Geological Survey Professional Paper 1173, 504 p.

McKee, E.D., and Gutschick, R.C., 1969, History of the Redwall Limestone of northern Arizona: Geological Society of America Memoir 114, 692 p.

McKee, E.D., Hamblin, W.K., and Damon, P.E., 1968, K-Ar age of lava dam in Grand Canyon: Geological Society of America Bulletin, v. 79, p. 133-136.

McKown, D.M. and Millard, H.T. Jr., 1987, Determination of uranium and thorium by delayed neutron counting, in Baedecker, P.A., ed., Methods for geochemical analysis: U.S. Geological Survey Bulletin 1770, p. I1-I12.

Miller, R.D., 1954, Copper-uranium deposits at the Ridenour mine, Hualapai Indian Reservation, Coconino County, Arizona, Pt. 1: U.S. Atomic Energy Commission Report RME-2014, 23 p.

O'Leary, R.M. and Meier, A.L., 1986, Analytical methods used in geochemical exploration: U.S. Geological Survey Circular 948, 48 p.

Roller, J.A., 1987, Fracture history of the Redwall Limestone and lower Supai Group, western Hualapai Indian Reservation, northwestern Arizona: U.S. Geological Survey Open-File Report 87-359, 33 p.

_____1989, Fracture history of the Redwall Limestone, lower Supai Group, and Tertiary units on the Hualapai Indian Reservation, northwestern Arizona: Additional data to Open-File Report 87-359: U.S. Geological Survey Open-File Report 89-463, 42 p.

Sutphin, H.B., and Wenrich, K.J., 1983, Structural control of breccia pipes on the southern Marble Plateau, Arizona: U.S. Geological Survey Open-File Report 83-908, 6 p., 2 plates, scale 1:50,000. (Superceded by U.S. Geological Survey Miscellaneous Investigations Series Map I-1778, 1988).

Sutphin, H.B., Wenrich, K.J., and Verbeek, E.R., 1983, Structural control of breccia pipes on the southern Marble Plateau, Arizona: Geological Society of America Abstracts with Programs, v. 15, no. 5, p. 376.

Taggart, J.E., Jr., Lindsay, J.R., Scott, B.A., Vivit, D.V., Bartel, A.J., and Stewart, K.C., 1987, Analysis of geologic materials by wavelength-dispersive X-ray fluorescence spectrometry, in Baedecker, P.A., ed., Methods for geochemical analysis: U.S. Geological Survey Bulletin 1770, p. E1-E19.

Verbeek, E.R., Grout, M.A., and Van Gosen, B.S., 1988, Structural evolution of a Grand Canyon breccia pipe: The Ridenour copper-vanadium-uranium mine, Hualapai Indian Reservation, Coconino County, Arizona: U.S. Geological Survey Open-File Report 88-006, 75 p.

Wenrich, K.J., 1985, Mineralization of breccia pipes in northern Arizona: Economic Geology, v. 80, no. 6, p. 1722-1735.

_____1986, Geochemical exploration for mineralized breccia pipes in northern Arizona, U.S.A.: Applied Geochemistry, v. 1, no. 4, p. 469-485.

Wenrich, K.J., Billingsley, G.H., and Huntoon, P.W., 1986, Breccia pipe and geologic map of the northeastern Hualapai Indian Reservation and vicinity, Arizona: U.S. Geological Survey Open-File Report 86-458A, 29 p., 2 plates, scale 1:48,000.

Wenrich, K.J., and Sutphin H.B., 1989, Lithotectonic setting necessary for formation of a uranium-rich, solution-collapse breccia-pipe province, Grand Canyon region, Arizona: U.S. Geological Survey Open-File Report 89-173, 41 p.

Wenrich, K.J., Sutphin, H.B., and Van Gosen, B.S., 1988, Distribution of Redwall Limestone-hosted breccia pipes across NW Arizona and the geochemistry and mineralogy of their orebodies: Geological Society of America Abstracts with Programs, v. 20, no. 7, p. A139.

Wenrich, K.J., Verbeek, E.R., Sutphin, H.B., Van Gosen, B.S., and Modreski, P.J., 1987, The Apex mine, Utah--A Colorado Plateau-type solution-collapse breccia pipe, in Sachs, J.S., ed., USGS research on mineral resources: U.S. Geological Survey Circular 995, p. 73-74, 76-77.

Wilson, S.A., Kane, J.S., Crock, J.G. and Hatfield, D.B., 1987, Chemical methods of separation for optical emission, atomic absorption spectrometry, and colorimetry, in Baedecker, P.A., ed., Methods for geochemical analysis: U.S. Geological Survey Bulletin 1770, p. D1-D14.

APPENDIX A

Samples collected from the Ridenour mine breccia pipe were analyzed using a variety of methods, including inductively coupled plasma-atomic emission spectroscopy (ICP-AES), X-ray fluorescence spectrometry, neutron activation, atomic absorption, and classical wet chemistry for specific elements or their anion complexes.

The ICP-AES technique uses a multi-acid digestion. A 0.2 gm sample is digested in hydrofluoric (HF), aqua regia, and perchloric ($HClO_4$) acids. The resulting solution is totally dried using a hot plate. The residue is dissolved in 1 ml of aqua regia and diluted to 10 gm using 1 percent nitric acid (HNO_3). This solution is then introduced into the ICP-AES instrument. Lutetium is used as an internal standard. The technique provides for the simultaneous analysis of 46 elements whose lower limits of determination are presented in table 1 below. This technique provides a precision of 10 percent relative standard deviation (RSD) for concentrations that are 10 times or more the detection limit (Lichte and others, 1987).

Detection limits for elements determined by ICP-AES
In ppm unless otherwise indicated
(from Lichte and others, 1987)

Element	Detection Limit	Element	Detection Limit
Ag	2	Mg	0.05%
Al	0.05%	Mn	10
As	10	Mo	2
Au	8	Na	0.1%
Ba	1	Nb	4
Be	1	Nd	20
Bi	10	Ni	2
Ca	0.05%	P	0.01%
Cd	2	Pr	10
Ce	4	Pb	4
Co	1	Sc	2
Cr	1	Sm	50
Cu	1	Sn	4
Dy	4	Sr	2
Er	4	Tb	20
Eu	2	Th	4
Fe	0.05%	Ti	0.01%
Ga	4	U	100
Gd	10	V	2
Ge	20	Y	2
Ho	4	Yb	1
K	0.1%	Zn	4
La	2		
Li	2		

All samples were analyzed by X-ray fluorescence spectrometry (XRF) for 9 major oxides--Al_2O_3, CaO, K_2O, MgO, MnO, Na_2O, P_2O_5, SiO_2, and TiO_2--using a method described by Taggart and others (1987). In this method 0.8 gm of sample is ignited in a tared platinum crucible at 925°C for 45 minutes and then cooled and weighed to determine loss on ignition (LOI, table 1). The weight loss is due to the volatilization of substances such as H_2O, CO_2, organic carbon, Hg, and Se. The ignited sample is then mixed with 8 gm of lithium tetraborate flux and fused at 1120°C for 40 minutes. The fused sample is then allowed to cool to a glass disk, which subsequently in exposed to an X-ray source in the XRF unit. The fluoresced X-rays emitted from the glass disc are then counted using a Philips PW1600 X-ray spectrometer. Inasmuch as problems can arise for samples containing more than 1 percent of metals, such as As and Pb, that alloy readily with the platinum crucible, such samples were not analyzed by X-ray fluorescence; these samples are designated "H" in the XRF data column, table 1. In some other samples the concentrations of As and Pb were sufficiently low that little damage would result to the crucible, but the concentrations of other heavy metals (particularly Cu at the Ridenour mine) were over 3 percent, resulting in problematical matrix effects. Consequently, major element totals for some samples deviated considerably from 100%. These samples are shown in table 1 with a parenthetical "H" before the data value.

Instrumental neutron activation analysis (INAA) was used to determine 26 elements in the Ridenour-mine samples. For INAA analysis 0.5-1.0 gm of powdered sample is weighed into a polyethylene vial and heat-sealed. The samples are then irradiated in a homogeneous neutron flux using the U.S. Geological Survey's TRIGA reactor. Two separate irradiations, of 8 hours each, are required for the analysis. After each irradiation the gamma rays emitted by each sample are counted using high-resolution coaxial Ge and LEPD detectors. Relatively long-lived (a few weeks to several years) indicator radionuclides, such as those of Sc, Co, and Fe, are counted 6 times, each of 1 to 2 hours duration over a 60 day decay period (Baedecker and McKown, 1987).

Delayed neutron activation analysis (DNAA) was used for the determination of U and Th (McKown and Millard, 1987). Approximately 10 gm of powdered sample is poured into a polyethylene vial, heat-sealed, and placed in a screw-capped polyethylene capsule for pneumatic transfer to a cadmium-lined irradiation terminus. After irradiation for 1 minute the sample is returned to the neutron counting assembly where, after a 5-second decay period, the neutrons are counted for 5 seconds and, after an additional 20 second delay, are counted for 60 seconds. The sample is then irradiated a second time using a bare irradiation terminus and returned for neutron counting using the same counting scheme as in the first cycle. Analytical precision is ± 5 percent for uranium concentrations of greater than 1 ppm in a 10-gm sample. A precision of ± 10 percent occurs for thorium where the Th-to-U ratio is greater than 3 and the thorium is present in concentrations of 10 ppm or greater (McKown and Millard, 1987).

All samples were analyzed for total carbon using a Leco CR-12 automated carbon analyzer with an IR carbon dioxide detector. About 0.75 gm of sample is combusted in an oxygen atmosphere at 1370°C, and the evolved CO_2 is determined (Jackson and others, 1987). Carbonate carbon is determined by digesting 0.1-0.5 gm of sample in 2-molar perchloric acid. The evolved CO_2 is collected in a coulometric cell where it is converted to an acid and titrated to a colorimetric end point (Jackson and others, 1987). Organic carbon is then determined by the difference between the total carbon and the carbonate

carbon. Reported mean relative standard deviations (RSD) (calculated from 2 to 4 replicate analyses of 19 marine shales) for the three forms of carbon--total, carbonate, organic--are 0.7, 2.0, and 1.6 percent, respectively (Jackson and others, 1987).

Total sulfur was determined using a Leco SC-132 automated analyzer. Approximately 0.25 gm of sample is combusted at 1370°C in an oxygen atmosphere with 1 gm of vanadium pentoxide flux. The evolved sulfur dioxide is measured using an IR detector. The lower limit of detection is reported at 0.01 percent (Jackson and others, 1987).

Samples were analyzed for fluorine by ion-selective electrodes (ISE). In this procedure 0.025 gm of sample is fused with sodium hydroxide and then dissolved in water. The solution is buffered to a pH of 6 using ammonium citrate. Fluorine is then determined with an ISE and a calibration curve. A RSD of 15 percent is reported for the described method with the limit of detection at 0.01 percent (Jackson and others, 1987).

Some samples from the Ridenour mine breccia pipe were analyzed for a variety of elements by atomic absorption spectrometry (designated AA in table 1). The various AA techniques generally are specific to single elements; for the sake of brevity the reader will be referred to the papers cited below for details. Gold was analyzed by atomic absorption spectrometry by digesting the sample in a hydrobromic acid-bromine solution followed by a methyl isobutyl ketone (MIBK) extraction (O'Leary and Meier, 1986). The relative standard deviation is 9.3 to 19.5 percent. Mercury was determined by cold-vapor atomic-absorption spectrometry with a relative standard deviation of 3.1 to 10.0 (Wilson and others, 1987). Arsenic and selenium were determined by hydride-generation atomic absorption spectrometry. The stated precision of the hydride technique is between ±2 to 15 percent (Wilson and others, 1987). Zinc was determined by atomic absorption spectrometry using a diethylene triamine pentaacetic acid extraction. The reported precision is 20 percent RSD for Zn concentrations exceeding the limit of detection by a factor of 15 or more (Wilson and others, 1987). Some samples were analyzed for Cs, Li, and Rb by atomic absorption spectrometry using the methods and associated digestion procedures described by Aruscavage and Crock (1987).

Some 18 elements, including Au, Ba, Ca, Ce, Co, Cr, Eu, Fe, K, La, Mg, Mn, Na, Nd, Th, Ti, U, and Zn, were determined by multiple methods; results for each method are shown in separate columns in table 1. Differences between methods in the apparent element concentrations of the same element may result from several factors (and combinations thereof): (1) Depending on the analytical technique or the chemical treatment used, the analysis may be partial or total; this could result from: (a) the acids not attacking and solubilizing all mineral forms in which an element is present; (b) the complexing of elements to form volatile species during digestion; or (c) the loss of the more volatile elements during the heating process of a particular digestion. (2) Most of the samples in table 1 contain elements in sufficiently high concentrations that problems of inter-element interferences or matrix effects commonly occur; these problems arise because the sample composition deviates significantly from the standards on which all inter-element interference corrections are based. Gone unchecked, this situation results in inaccurate corrections which may artificially enhance or reduce reported element concentrations. (3) Mechanical problems may exist where: (a) the sample aliquot taken for a particular test may not be representative of the whole sample due to sample inhomogeneity or a "nugget effect", which is particularly prevalent with elements such as Au, Ag, or Cu; (b) weighing errors during chemical preparation; (c) instrument drift during analysis, (d)

nonreproducible positioning of the sample during counting; and (e) extended spectral overlap due to high excitation energy emitted from the source.

There is one "replicate" sample in the data set of samples from the Ridenour mine breccia pipe. The "replicates" are designated 223-W-C86 and 223-W-C86R. Unfortunately the sample was split in half prior to grinding and it is possible that, considering the trace metal enrichment of this sample, that some metal-rich minerals were preferentially concentrated in one or the other of the two splits. Review of the data from the analysis of these "replicates" suggests that perhaps this is the case and the replicate was not homogeneous split of the same sample. Because it is uncertain that 223-W-C86 and 223-W-C86R are true analytical replicates, little can be said for certain about the precision of the data in table 1. All that can be concluded is that the variance in the data is either due to (1) poor data precision, (2) a large concentration range of many elements, which has resulted from inhomogeneity in the mineralized rock at the Ridenour mine, or (3) a combination of both.

APPENDIX B
Petrographic description
of samples collected at the Ridenour mine.
* = analyzed sample (table 1)

223-A-C82* Dark-grayish-brown, very fine grained quartz sandstone.

89% Detrital framework grains
- 89% monocrystalline quartz - subrounded to very angular, 0.08-0.15 mm diameter
- <1% polycrystalline quartz - subrounded to very angular, 0.08-0.15 mm diameter
- Trace microcline - unaltered, tabular, 0.1-0.2 mm in length
- Trace heavy mineral suite - tourmaline, zircon

<1% Pore space

11% Matrix[1]
- 10% roscoelite - microcrystalline, surrounding all framework grains. More abundant in microfractures with metatyuyamunite
- <1% metatyuyamunite - minor amounts, poorly crystalline, scattered in matrix and concentrated along microfractures
- Trace malachite - rimming quartz grains

Texture
- Majority of framework grains are floating; minor long and point contacts. Unimodal; very well sorted

Mineralization/alteration
- Roscoelite matrix is probably secondary, having replaced the original carbonate (calcite?). It is more abundant along and in the vicinity of microfractures that host metatyuyamunite.
- In one area malachite-rimmed quartz grains are contained within the roscoelite matrix.

223-AA-C86* Black, very fine to fine grained quartz sandstone.

92% Detrital framework grains
- 91% monocrystalline quartz - subrounded to angular, 0.09 mm diameter; a few erratic grains 0.2 mm diameter
- Trace chert
- Trace plagioclase - well rounded
- <1% heavy mineral suite - tourmaline, zircon, pyroxene. Altered oxides of Fe and Ti
- Trace rock fragments - (metamorphic) schistose quartz grains

<1% Pore space

8% Matrix
- >7% roscoelite - microcrystalline, comprises 100% of the matrix in most of the section
- Trace malachite
- Trace sericite - in a halo area around a spot containing hematite matrix
- <1% hematite - isolated area with 100% hematite matrix

Texture
- Mixture of grains having floating, long and point contacts, very well sorted.

[1]"Matrix" includes all finer-grained material that encloses the larger, detrital grains.

223-AA-C86 continued

Mineralization/alteration

Roscoelite matrix is probably not original or diagenetic.
Minor replacement of the framework quartz by hematite occurred in the area containing the hematite matrix. The edges of all the quartz grains are serrated and embayed by the hematite.

223-AB-C86 4 in. diameter "goethite" nodule with a friable limonitic core and spots of malachite and azurite.

25% Detrital framework grains

24% monocrystalline quartz - subrounded to subangular, 0.08-1.5 mm diameter
Trace polycrystalline quartz
<1% chert
1% K-feldspar - tabular to equant, visible cleavage, unaltered
Trace microcline
Trace muscovite - small flakes, 0.05 mm long

5% Pore space - porous matrix goethite

70% Matrix

5% hematite
2% limonite
61% goethite - microscopic boxwork goethite, highly porous
1% sericite - in area of matrix that lacks goethite
<1% microcrystalline quartz - in area of matrix that lacks goethite
1% malachite - locally filling goethite boxwork pores

Texture

Floating detrital grains in goethite. Center of nodule and areas without goethite are more friable.

Mineralization/alteration

No remnant pyrite or any other indication of a precursor to the goethite.
Malachite was deposited in the pore spaces of the goethite boxwork.

223-B-C83 Light- to dark-gray, very fine grained, dolomitic quartz sandstone, with splotches of volborthite, malachite, and tyuyamunite.

75% Detrital framework grains

<75% monocrystalline quartz - angular to very angular, 0.05-0.15 mm diameter
<1% chert
Trace polycrystalline quartz
Trace muscovite - 0.09 mm long, unaltered
Trace heavy minerals - leucoxene, rutile, tourmaline

<1% Pore space

25% Matrix

14% dolomite - euhedral rhombs up to 0.35 mm across, each enclosing several quartz grains. Also clusters of rhombs
9% roscoelite - microcrystalline, imparting dark color to the rock
<1% volborthite - anhedral, also scattered throughout the matrix
Trace malachite - fibrous
Trace tyuyamunite - poorly crystallized
2% sericite

223-B-C83 continued

Texture

Floating framework grains, slight embayment of dolomite by roscoelite. Poikilotopic dolomite crystals enclosing framework quartz.

Mineralization/alteration

Roscoelite, malachite, volborthite, ± tyuyamunite

223-D-C83* Mottled, red-to-white-to-black, very fine grained, slightly calcareous quartz sandstone.

97% Detrital framework grains

96% monocrystalline quartz, subrounded to subangular, 0.1 mm diameter
<1% polycrystalline quartz
<1% chert
Trace orthoclase - tabular to equant, minor alteration along cleavage
Trace plagioclase - tabular to equant, minor alteration
<1% muscovite - slightly bent, thin flakes and thicker unbent flakes, 0.1 mm long
Trace heavy minerals - tourmaline, zircon, opaques, riebeckite

Trace Pore space

3% Matrix

1% calcite - spotty occurrences. Each spot engulfing 10-20 quartz grains
1% hematite - disseminated and as halos around detrital oxides of Fe and Ti
1% sericite - borders around framework grains
Trace metatyuyamunite - well-formed "square-equant" crystals, some transparent, most translucent

Texture

Straight and concavoconvex quartz grain contacts; very well-sorted

Mineralization/alteration

Metatyuyamunite and minor hematite concentrated in the same pores.
Trace amounts of galena, pyrite, and marcasite. 4-5 small galena crystals or cubic cleavage fragments. Pyrite grains are smaller and rather anhedral; may be detrital. One euhedral marcasite crystal.

223-E-C83* Gray-black, very fine grained quartz sandstone with disseminated dots of tyuyamunite. Section taken perpendicular to a fracture surface. Color fades from black to gray with increased distance from the fracture. Sample from along a ring fracture.

85% Detrital framework grains

80% monocrystalline quartz - subrounded to very angular, 0.06-0.11 mm diameter
5% polycrystalline quartz
<1% plagioclase - subrounded, unaltered
Trace microcline - very minor alteration along cleavage
Trace orthoclase - very minor alteration along cleavage
<1% muscovite - 0.15 mm long, undeformed

223-E-C83 continued

<1% heavy minerals - pyroxene, tourmaline, oxides of Fe and Ti

<1% Pore space

15% Matrix

Trace dolomite - a few scattered rhombs
>4% roscoelite - microcrystalline
<1% sericite
Trace microcrystalline quartz
<1% tyuyamunite and volborthite

Texture

Unimodal, well sorted. Gradational from floating grains to long and point contacts with increased distance from fracture. Angularity of quartz is partially secondary due to corrosion by roscoelite.

Mineralization/alteration

Tyuyamunite, volborthite and roscoelite. Roscoelite is by far most abundant. Several things happen with increased distance from the fracture: (1) rock color lightens, (2) roscoelite amount decreases, (3) matrix percentage decreases as the framework grains get closer together, and (4) quartz grains are less corroded. All this implies the roscoelite was introduced along the fracture and migrated outward into the sandstone.

223-F-C86 Pale-gray, very fine to fine-grained quartz sandstone with spot occurrences of tyuyamunite. (This sample is a resampling of 223-F-C83)

96% Detrital framework grains

93% monocrystalline quartz - detrital shape is subangular to rounded. All grains have extensive quartz overgrowths, 0.08-0.15 mm diameter
2% polycrystalline quartz
<1% plagioclase - minor alteration along cleavages and grain edges, ~0.13 mm diameter
Trace orthoclase
Trace muscovite - a few bent flakes
<1% heavy minerals - rutile, tourmaline

1% Pore space

Incompletely filled space between junctions of adjacent quartz overgrowths

3% Matrix

>2% quartz overgrowths
Trace carbonate
Trace sericite

Texture

Unimodal, equicrystalline mosaic, straight to curved contacts between adjacent overgrowths.

Mineralization/alteration

Microfractures filled with tyuyamunite (radial, fibrous, translucent) tufts and coarsely crystalline calcite.

223-F-C83* Buff gray, very fine to fine grained quartz sandstone with disseminated metatyuyamunite and scattered dots of hematite.

95% Detrital framework grains
- 93% monocrystalline quartz - 0.5-0.17 mm diameter, subrounded to angular
- 1% polycrystalline quartz
- <1% plagioclase - unaltered
- Trace microcline - altered
- Trace orthoclase - some very altered
- <1% muscovite - thin undeformed plates
- Trace heavy minerals - glauconite, tourmaline, zircon, pyroxene

<1% Pore space

5% Matrix
- 3% quartz overgrowths - irregular, sutured with adjacent overgrowths
- 1% dolomite - scattered rhombs each enclosing several framework grains
- 1% sericite
- Trace roscoelite

Texture
- Unimodal, equicrystalline mosaic, mostly curved contacts with minor suturing.

Mineralization/alteration
- Minor metatyuyamunite in intergranular pore space.

223-G-C83* Gray, very fine grained, calcareous quartz sandstone with minor hematite mottling.

80% Detrital framework grains
- 78% monocrystalline quartz - subrounded-angular, 0.06-0.12 mm
- 2% polycrystalline quartz
- Trace chert - 0.17 mm
- <1% orthoclase
- <1% plagioclase - rounded
- Trace microcline
- <1% muscovite - frayed flakes
- Trace heavy minerals - amphibole, leucoxene

<1% Pore space

20% Matrix
- 19% recrystallized calcite - syntaxial crystals ~3 mm diameter
- <1% roscoelite
- Trace goethite
- Trace hematite

Texture
- Well sorted, point contact framework, some floating grains in larger matrix calcite crystals.

Mineralization/alteration
- Roscoelite.
- Later fracturing followed by fracture-lining hematite and fracture-filling calcite.

223-I-C83 Breccia. Silty, very fine to fine grained quartz sandstone clasts in malachite matrix.

Sandstone clasts

89% Detrital framework grains
- 80% monocrystalline quartz - subrounded to angular, <0.06-0.15 mm diameter
- 5% polycrystalline quartz
- <1% chert
- <1% plagioclase - unaltered
- 2% orthoclase - unaltered
- Trace microcline
- Trace muscovite - frayed fibers
- <1% heavy mineral suite - pyroxene, tourmaline, rutile
- 1% rock fragments - schistose quartz grains

<1% Pore space

11% Matrix of the sandstone
- 5% dolomite - poikilotopic crystals
- 2% sericite - surrounds most grains
- Trace miscellaneous clays
- 4% microcrystalline quartz

Texture

Concavo-convex contacts of adjacent quartz grains in sandstone clasts, unimodal, minor corrosion of framework grains by sericite formation; well sorted.

Mineralization/alteration

Brecciation; mechanical plucking/ entrainment/disaggregation of framework grains from the host sandstone; some fractures show cataclastic deformation. Hematite and malachite mineralization. Very minor amounts of acanthite in the thickest portion of the breccia matrix. Matrix is very porous as shown by the small, incompletely filled "micro-vugs" lined by crystalline malachite.

223-I1-C86 Ring fracture breccia - pink, sandy, isolated clasts floating in a matrix of Cu-bearing minerals.

The host sandstone or breccia clasts consist of ~40% very fine grained quartz framework grains, all floating in a coarsely recrystallized calcite matrix. Individual matrix calcite crystals are ~0.5 mm diameter. The breccia clasts also contain scattered "spots" of malachite and goethite. Microfractures were successively lined with goethite, malachite, and calcite.

The breccia matrix contains ~5% disaggregated quartz grains. The rest is 80% malachite, 12% sulfides (covellite, digenite, chalcocite, pyrite), 2% hematite, and 1% pore space.

This section also contains one spot occurrence (3 mm x 1 mm) of a dendritic oxide of Mn, Fe, or possibly Co within the breccia clast.

Malachite from the breccia matrix partially penetrates or "bleeds" into the outer edge of the breccia clast.

223-I2-C86 Vuggy calcite and malachite fracture-fill.

Crystalline calcite (85% of section) on boxwork goethite host, similar to 223-M1-C86 (described below). Calcite crystals contain syngenetic intergrowths of dendritic hematite. Malachite prisms arranged in radial tufts occur with the innermost band of calcite crystals which line small vugs. Some of the larger malachite tufts also contain intergrown hematite.

One part of the section contains a translucent to opaque area composed of a finer network of boxwork goethite and hematite. Most of the cells are filled with malachite. Some of the cells are completely to partially filled with digenite and covellite.

At the edge of this translucent part of the section is a 1 mm square area that contains square and hexagonal, crystalline goethite shapes with smaller hallow cores. These are strongly suggestive of precursor pyrite crystals having bravoite cores.

223-L-C86 Fracture-filling carbonate and Cu-bearing minerals, along with embedded and partially altered fragments derived from the adjacent host sandstone.

Host-rock fragment is a sandy sparite. 35% monocrystalline quartz, 0.05-0.15 mm diameter, subrounded to angular. All grains are floating in a coarsely crystalline calcite matrix which contains variable amounts of malachite.

Fracture-fill material is mostly translucent (brownish green) and for the most part in an intermediate stage of alteration between the precursor fracture-filling sulfides (irregular remnants of pyrite, digenite, and covellite are still present) and malachite which stains the section and fills small pores and vugs. Malachite bleeds inward from the fracture material into the host-rock fragment. At the edge of the clasts, the calcite matrix of the interior of the clasts is completely replaced by a matrix of malachite.

A late-stage calcite fills fractures that cut the malachite and Cu-sulfide fracture fill.

223-M1-C86* Crystalline, vuggy, boxwork calcite.

10% thin boxwork goethite
80% crystalline calcite
10% open space (vugs)

The thin boxwork goethite provided the framework for the later calcite to deposit on. Calcite crystals radiate outward from the goethite fins. Calcite crystal size increases away from the goethite fins in a typical open-space-filling texture.

223-M2-C86 Mottled blue, yellow, gray, and dark-red, very fine grained quartz sandstone.

<u>80% Detrital framework grains</u>

78% monocrystalline quartz - subrounded to angular, 0.08-0.12 mm diameter
2% polycrystalline quartz
<1% muscovite - undeformed, some slightly bent flakes
Trace heavy mineral suite - pyroxene, tourmaline

223-M2-C86 continued

3% Pore space

Lined by illite (formed by feldspar alteration?)

17% Matrix

10% roscoelite
5% illite - with some kaolinite?
>1% dolomite - isolated crystals
1% azurite
<1% volborthite
Trace tyuyamunite
Trace malachite

Texture

Unimodal, point and straight contacts. Some floating grains, especially those surrounded by roscoelite. Well sorted.

Mineralization/alteration

Disseminations throughout the matrix of azurite, malachite, volborthite, and tyuyamunite result in the mottled-color appearance of the sample. Roscoelite produces the overall dark grey appearance and is present throughout. Dolomite seems to be mutually exclusive of the colored ore minerals.

Unlike all other sandstone sections, not one grain of feldspar is present. It appears that all of the feldspar has been thoroughly altered to illite, which lines large pores that are reminiscent of previous framework grains. Illite has also been added to the section as there is quite a bit more present than would result from altering <2% feldspar.

Associated with the illite are trace amounts of an unidentified mineral. <0.01 mm in diameter, translucent, deep amber-colored crystals.

223-N1-C86* Gray, very fine grained sandstone, impregnated with secondary copper-bearing minerals, especially concentrated on open fracture faces.

90% Detrial framework grains

88% monocrystalline quartz - subrounded to subangular, 0.1-0.15 mm diameter
1% polycrystalline quartz
<1% plagioclase - minor alteration along twin planes
Trace microcline - partially altered along twins
Trace muscovite - flakes bent around adjacent grains
Trace heavy mineral suite - tourmaline, zircon, pyroxene

<1% Pore space

10% Matrix

1% sericite
<1% roscoelite
5% malachite
1% acanthite
2% tyuyamunite
1% calcite
Trace azurite

223-N1-C86 continued

Texture

Well-sorted; slight alignment of elongated detrital grains; concavoconvex and straight contacts between quartz grains. Floating grains in the area of malachite matrix.

Mineralization/alteration

Spotty concentrations of malachite through the matrix. Zoned malachite and tyuyamunite, banded parallel to the fracture surfaces. Microfractures filled with dense malachite, which contains residual corroded specks of acanthite.

Several 0.5 mm long barite molds are present--most are empty. One is filled and another is partially filled with either calcite or dolomite.

223-P-C86* Color banded, very fine to fine grained quartz sandstone.

95% Detrital framework grains

94% monocrystalline quartz - 0.06-0.13 mm diameter, subrounded to angular

<1% polycrystalline quartz

1% plagioclase - alteration along cleavages

Trace microcline

Trace muscovite

Trace rock fragments - metamorphic

<1% heavy mineral suite - tourmaline, rutile

<1% Pore space

5% Matrix

1% chert

4% variably zoned azurite, malachite, roscoelite, tyuyamunite

Texture

Minor fluxion structure throughout section. Cataclastic sheared zones are heavily mineralized. En echelon fractures at ~60° to sheared zones are filled with malachite.

Mineralization/alteration

Sheared and fractured sandstone. Pervasive fracturing through quartz framework grains.

Minor chalcocite, also localized naumannite and acanthite.

Color zonation parallel to rock fabric, primarily azurite, malachite, roscoelite, and minor tyuyamunite.

223-Q-C86* Light-tan, very fine grained, calcareous quartz sandstone, with spotty tyuyamunite impregnations and volborthite-filled fractures.

45% Detrital framework grains

<45% monocrystalline quartz - rounded to subangular, 0.6-0.13 mm diameter

Trace plagioclase - unaltered

Trace muscovite - very thin, fibrous

Trace Pore space

55% Matrix

55% carbonate - mostly calcite, but some obvious dolomite

223-Q-C86 continued

Texture

Floating quartz grains in equigranular crystalline carbonate matrix.

Mineralization/alteration

Spot replacement of matrix by tyuyamunite. Successive open-space fracture filling by azurite, volborthite, and dolomite.

223-S-C86* Dark, multicolored (black, blue, green, yellow) siltstone to very fine grained quartz sandstone, with heavily mineralized fractures.

93% Detrital framework grains

<92% monocrystalline quartz - very angular to subrounded, some shard-like, <0.05-0.1 mm diameter

1% polycrystalline quartz

<1% highly altered grains - presumably feldspar

<1% muscovite - slightly bent and frayed

Trace heavy minerals - pyroxene

<1% Pore space

7% Matrix

Mineralized and composed of disseminated malachite, volborthite, roscoelite, hematite, azurite, and irregular corroded opaque sulfides.

Texture

Unimodal quartz with minor point contacts, mostly floating in matrix mineral assemblage. Relatively minor corrosion of quartz with the local exception of severe corrosion by an unknown Cu-As-V mineral.

Mineralization/alteration

Fracture filled with corroded remnant "islands" of (1) digenite with small pyrite inclusions and rinds of covellite, and (2) covellite grains (that completely replaced digenite). Brochantite, malachite, azurite, volborthite, tyuyamunite, barite (in hand sample), and roscoelite also fill fractures. In the vein, roscoelite surrounds the sulfide fragments just as it does the sandstone framework grains.

All of the fracture-fill minerals are present in variable amounts in the sandstone matrix, especially the malachite and V-minerals. The sandstone matrix also contains equant, hexagonal, green crystals (0.02 mm diameter) of an unknown Cu-As-V mineral. The digenite and especially the covellite are intergrown with naumannite and acanthite. These silver-bearing minerals also occur by themselves and have a very irregular, corroded morphology.

223-T-C86* Pink, very fine to fine grained, calcareous quartz sandstone.

40% Detrital framework grains

<40% monocrystalline quartz - 0.07-0.2 mm diameter, subrounded to subangular

Trace chert

Trace microcline

Trace orthoclase

223-T-C86 continued

Trace muscovite - 1 mm in diameter, undeformed.
Trace heavy mineral suite - rutile, tourmaline

Trace Pore space

60% Matrix

58% carbonate - mostly dolomite, but intermixed with some calcite. Matrix crystals up to 2 mm diameter
2% hematite - pigment and intergranular pore filling

Texture

Variable--both tightly packed grain-supported, and matrix supported with floating clastic grains. The rock is matrix supported within the individual poikilotopic matrix carbonate crystals, but becomes grain supported along boundaries between adjacent matrix carbonate crystals.

Mineralization/alteration

None

223-U1-C86* and 223-U2-C86*

Silty to fine grained, sandy, calcareous mudstone, with mottled hematite staining.
"Mud crack" filling in the Esplanade?

223-V-C86 Pale-orange quartz sandstone with goethite and calcite fracture fillings.

45% Detrital framework grains

43% monocrystalline quartz - rounded to angular, <0.03-0.15 mm diameter
1% polycrystalline quartz
<1% plagioclase
<1% muscovite
Trace heavy mineral suite

Trace Pore space

55% Matrix

2% sericite
3% microcrystalline quartz
50% carbonate - coarsely crystalline, 0.5 mm diameter

Texture

Poorly sorted, floating framework grains

Mineralization/alteration

Fractures lined by goethite and filled by calcite

223-W-C86* and 223-W'-C86 Variably mottled, black to yellow, very fine to fine grained quartz sandstone.

82% Detrital framework grains

80% monocrystalline quartz - rounded to angular, <0.1-0.15 mm diameter
2% polycrystalline quartz
<1% chert
Trace muscovite - bent flakes, frayed ends
Trace heavy mineral suite

223-W-C86 and 223-W'-C86 continued

<1% Pore space
18% Matrix
2% microcrystalline quartz
15% roscoelite
<1% volborthite - transparent yellow
<1% tyuyamunite - translucent, radially fibrous, yellow
Texture
All grains bordered by roscoelite rinds; slightly corroded quartz grain margins; moderately well-sorted.
Alteration/mineralization
Roscoelite throughout matrix. Fractures successively filled by volborthite and tyuyamunite.

223-Y-C86* and 223-Y'-C86 Mineralized vein material with parallel bands of azurite and malachite staining the adjoining sandstone.

Host sandstone is a very fine to fine grained quartz sand with mainly straight and slightly undulatory grain contacts. The matrix is all secondary (~7% total volume) and is zoned in bands parallel to the main mineralized fracture. Outward matrix zoning over 3/4 inch of section is malachite, hematite/goethite, azurite, malachite.

The vein-filling material contains ~10% disaggregated quartz grains suspended within malachite (45%). Also surrounded by malachite are corroded islands of sulfide minerals, the source for the Cu in the malachite. The most abundant sulfide is digenite (36%). Digenite contains small flecks (<1%) of pyrite, is being altered to covellite (~5%), and occurs with or is intergrown with acanthite (1%). Two bornite grains (<1%) are intergrown with chalcopyrite (Trace) and have alteration rinds of digenite. Chalcocite (<1%) and hematite (2%) are also dispersed in the vein.

A second stage of fracturing and mineralization (or redistribution of previously deposited Cu phases) is shown by small malachite-filled fractures that cut the earlier-formed vein minerals.

223-Z-C86 Fine grained, mottled pink to white, quartz sandstone.
97% Detrital framework grains
96% monocrystalline quartz - 0.11-0.17 mm diameter, subrounded to subangular
Trace chert
<1% plagioclase
Trace muscovite
<1% heavy mineral suite
0% Pore space
3% Matrix
1% hematite after pyrite cubes - euhedral, 0.010-0.015 mm diameter
<2% dolomite - poikilotopic rhombs 0.5-1 mm diameter
<1% sericite

223-Z-C86 continued

Texture

Well-sorted, equigranular mosaic. Concavo-convex contacts between adjacent quartz grains. Matrix-supported, floating quartz grains only where dolomite is present.

Mineralization/alteration

Distribution of minute hematite cube-like shapes occur in the variable pink to white mottling of the sandstone.

223-Z1-C86* Light- to dark-gray, dolomitic quartz siltstone to very fine grained sandstone.

80% Detrital framework grains

<80% monocrystalline quartz - subrounded to subangular, 0.04-0.1 mm diameter
Trace polycrystalline quartz - subrounded to subangular, 0.04-0.1 diameter
Trace chert
Trace muscovite - slightly frayed, 0.1-0.2 mm diameter
Trace heavy minerals - tourmaline

<1% Pore space

20% Matrix

13% dolomite - poikilotopic crystals, pre-roscoelite, ~0.3 mm diameter
7% roscoelite
<1% volborthite - crystalline and minor staining of dolomite
Trace goethite

Texture

Well sorted. Floating grains in dolomite. Point contact grains in roscoelite matrix.

Mineralization/alteration

Dolomite may be original cement.
Volborthite, spotty, occurs within denser patches of roscoelite.

223-Z2-C86 Bleached siltstone to very fine grained sandstone with fracture fillings and impregnations of secondary Cu, V minerals.

90% Detrital framework grains

89% monocrystalline quartz - 0.05-0.11 mm diameter, rounded to angular
<1% microcline
<1% plagioclase
Trace muscovite - slightly bent
Trace heavy mineral suite - glauconite, tourmaline

<1% Pore space

10% Matrix

Variable percentage of each mineral depending on location in the section. Composed of azurite, illite, halloysite, goethite, malachite, roscoelite, and vesignieite.

223-Z2-C86 continued

Texture

Originally tightly packed, now the framework grains are all separated by the secondary matrix minerals (likely due to both displacive growth of new minerals and the less common replacement of original detrital grains). Framework well-sorted.

Alteration/mineralization

All of the above-listed matrix minerals are secondary, including illite and halloysite.

Fracture filling by crystalline volborthite, vesignieite, and malachite.

Denser areas of azurite contain highly altered semi-opaque sulfides in which only minute specks of digenite are distinguishable.

223-ZZ-C86* Goethitic, very fine to fine grained quartz sandstone with scattered azurite.

91% Detrital framework grains

Monocrystalline quartz - subrounded to angular, 0.07-0.18 mm diameter

<1% polycrystalline quartz

1% chert

Trace microcline

<1% orthoclase

<1% muscovite

Trace Pore space

7% Matrix

2% azurite - filling intergranular pore space

3% goethite/hematite - botryoidal aggregates

1% illite - pore lining

<1% halloysite - pore filling

Trace local euhedral quartz overgrowths

Trace roscoelite

Texture

Well sorted and unimodal. Most framework grains are floating or separated from adjacent grains by the secondary matrix minerals. Less mineralized portions still have straight grain contacts.

Mineralization/alteration

Replacement of original matrix by azurite, malachite, roscoelite, goethite, halloysite, and illite.

APPENDIX C

Microprobe analyses of volborthite, calciovolborthite, naumannite, argentite, calcite, an unidentified Cu-arsenate and an unidentified black Co-Cu Oxide

MICROPROBE ANALYSIS - RIDENOUR VOLBORTHITE
sample 223-S-C86

oxide	ideal wt.%	analysis avg. of 2	atomic proportions (8 ox.)	
CuO	50.29	48.33	Cu	2.870
CaO	-	0.05	Ca	0.004
FeO	-	0.38	Fe	0.025
V_2O_5	38.33	38.35	V	1.992
As_2O_5	-	1.18	As	0.048
H_2O	11.39	-		
total	100.01	88.29	O	7.999

calculated formula (assumed 3 H_2O):

$(Cu_{2.87}\ Fe_{0.03})_{2.99}\ [(VO_4)_{1.99}\ (AsO_4)_{0.05}]_{2.04} \cdot 3H_2O$

MICROPROBE ANALYSIS - RIDENOUR CALCIOVOLBORTHITE
sample 223-S-C86

oxide	ideal wt.%	analysis avg. of 2	atomic proportions (4.5 ox.)	
CaO	23.81	22.69	Ca	1.061
CuO	33.77	32.32	Cu	1.061
FeO	-	0.29	Fe	0.010
V_2O_5	38.60	24.02	V	0.692
As_2O_5	-	11.10	As	0.253
H_2O	3.82	-		
total	100.00	90.42	O	4.495

calculated formula [assumed 1 (OH)]:

$Ca_{1.06}\ Cu_{1.06}\ Fe_{0.01}\ [(VO_4)_{0.69}\ (AsO_4)_{0.25})]_{0.94}\ OH$

Microprobe analyses: ARL-SEMQ microprobe; 20 keV accelerating voltage; 64 nA beam current; 10 nA sample current; counting times 20 seconds on peak, 20 seconds each on high and low background positions; standards: olivenite (Cu,As); volborthite (V); hematite (Fe); wollastonite (Ca); matrix correction by MAGIC-IV.

SEMIQUANTITATIVE MEASUREMENT OF Cu CONTENT
OF NAUMANNITE AND ARGENTITE, RIDENOUR MINE
sample 223-S-C86

grain no. and size	weight percent Cu
naumannite #1, 10 μm	5 %
" #2 20 μm	1 %
" #3, 20 μm	2 %
" #4, 20 μm	4 %
argentite #1, 20 μm	3.5 %

Microprobe analysis, 20 keV; Ag_2S and Cu metal standards; no matrix corrections. No other elements besides major Ag and Se were detected in naumannite, $(Ag,Cu)_2Se$; trace Se (0.5 weight percent) was detected in the argentite, $(Ag,Cu)_2S$.

RIDENOUR MINE - MICROPROBE ANALYSES
CAVITY-FILLING CALCITE

	sample 223-I2-C86					sample 223-M1-C86			
	std. dev.	anal. 1	anal. 2	avg. of 2	as[1] MCO3	anal. 1	anal. 2	avg. of 2	as[1] MCO_3
MgO	0.04	0.38	0.56	0.47	0.98	0.32	0.29	0.30	0.63
CaO	0.63	54.77	54.89	54.83	97.86	54.58	55.18	54.88	97.95
MnO	0.09	0.00	0.04	0.00	0.00	0.16	0.23	0.20	0.32
FeO	0.12	0.00-	0.15	0.00	0.00	0.00-	0.20	0.05	0.08*
SrO	0.05	0.10	0.08	0.09	0.13	0.00-	0.00-	0.00	0.00
sum	-	55.25	55.72	55.39	98.97	55.06	55.90	55.43	98.98

(-) after value = nominal computed concentration of component from microprobe analysis is negative (measured peak counts are less than background counts); the value in the average column for this component is reported as the vector sum of measured positive and negative concentrations (zero if the sum is negative), to better take into account the observed range of variation in analytical measurements.
(*) = reported average concentration is less than the estimated standard deviation based on counting statistics; the reported value could be zero within the expected range of statistical variation.

Microprobe analysis on ARL-SEMQ electron microprobe, April 1988; 10 KeV accelerating voltage; 32 nA beam current; 5 nA sample current; counting times, 20 seconds on peak, 4 seconds each on high and low background positions. Matrix corrections by MAGIC-IV program; standards: calcite (Ca), dolomite (Mg), rhodochrosite (Mn), siderite (Fe), celestite (Sr).

[1]"As MCO_3" = analytical averages converted from divalent oxide to divalent carbonate weight percent, assuming that each metal is present as an $M^{2+}CO_3$ component. Ideal calcite = 56.03 weight percent CaO, 100.00 weight percent $CaCO_3$.

MICROPROBE ANALYSIS - UNIDENTIFIED CU-ARSENATE, RIDENOUR MINE SAMPLE 223-S-86
15-30 MICRON HEXAGONAL-SHAPED GREEN CRYSTALS INCLUDED IN QUARTZ

	grain 1 20 µm hexagons avg. of 3 anal.	grain 2 15 µm hexagons avg. of 2 anal.	grain 3 25 µm hexagons avg. of 2 anal.	grain 4 anhedral 1 anal.	ideal compositions (I)	(II)	(III)	(IV)
CuO	60.32	59.87	58.96	60.28	62.70	59.94	58.35	56.21
CaO	0.31	0.35	0.33	0.37	-	-	-	-
FeO	3.29	3.27	3.83	3.31	-	-	-	-
As_2O_5	25.94	26.28	26.79	26.98	30.20	34.63	33.72	40.61
V_2O_5	5.57	5.34	5.21	5.15	-	-	-	-
H_2O	n.m.	n.m.	n.m.	n.m.	7.10	5.43	7.93	3.18
total	95.43	95.11	95.12	96.09	100.00	100.00	100.00	100.00
atomic proportions (normalized to 12 total metal atoms)								
Cu	8.298	8.272	8.154	8.253	9.000	8.571	8.571	8.000
Ca	0.060	0.069	0.065	0.072	-	-	-	-
Fe	0.501	0.500	0.586	0.502	-	-	-	-
As	2.470	2.513	2.565	2.557	3.000	3.429	3.429	4.000
V	0.670	0.645	0.630	0.616	-	-	-	-
total	11.999	11.999	12.000	12.001	12.000	12.000	12.000	12.000
atomic ratio (Cu+Ca+Fe)/(As+V) for the above analyses and minerals:								
	2.821	2.800	2.756	2.781	3.000	2.500	2.500	2.000

Microprobe analysis: ARL-SEMQ microprobe; 20 keV accelerating voltage; 64 nA beam current; 10 nA sample current; counting times, 20 seconds on peak, 20 seconds each on high and low background; standards: olivenite (Cu,As), volborthite (V), hematite (Fe), wollastonite (Ca); matrix correction by MAGIC-IV. n.m. = not measured (H_2O). Also looked for but not detected: Na, Mg, Zn. Ideal compositions for comparison: (I) = clinoclase, $Cu_3(AsO_4)(OH)_3$; (II) = cornubite, $Cu_5(AsO_4)_2(OH)_4$; (III) = cornwallite, $Cu_5(AsO_4)_2(OH)_4.H_2O$; (IV) = olivenite, $Cu_2(AsO_4)OH$.

BLACK Co-Cu OXIDE, RIDENOUR MINE
SEMIQUANTITATIVE ANALYSIS

Approximate analysis using Tracor-Northern "SQ" spectrum-fitting program; energy-dispersive X-ray analyzer on Cambridge Stereoscan 250 Mk2 scanning electron microscope; 20 kV accelerating voltage. Composition is given as the total of anhydrous components summed to 100%. V is arbitrarily expressed as V_2O_3, and Fe as FeO.

Sample 223-X-C86

	#1	#2	#3	#4	avg. of 4
MgO	2.2	2.5	1.7	1.5	2.0
Al_2O_3	0.5	2.8	5.1	4.0	3.1
SiO_2	1.4	5.0	2.6	2.2	2.8
CaO	6.1	1.3	1.9	2.0	2.8
TiO_2	0.1	0.3	0.0	0.0	0.1
V_2O_3	3.6	3.6	3.1	3.7	3.5
MnO	0.0	0.0	0.4	0.1	0.1
FeO	0.2	0.1	0.2	0.0	0.1
CoO	73.3	71.6	72.0	73.7	72.7
CuO	11.2	12.8	12.6	11.9	12.1
ZnO	1.4	0.0	0.0	0.8	0.5
BaO	0.0	0.1	0.3	0.0	0.1
total	100.0	100.1	99.9	99.9	99.9

Approximate semiquantitative analysis of same sample by KEVEX energy-dispersive X-ray fluorescence spectrometry (analysis of bulk sample including some sandstone matrix plus fracture-filling calcite); weight percent element:

	Ca	V	Fe	Co	Cu	As	Rb	Sr	Y	Zr
anal. 1	9	4	3	30	6	0.4	0.4	0.6	0.15	0.9
anal. 2	6	2	2	30	4	0.5	0.2	0.3	0.1	0.9

[Cobalt content was assumed to be 30 wt.%, and concentrations of all other components are normalized relative to this assumed concentration.]